Petrology, Vol. 8, No. 2, 2000, pp. 177–199. Translated from Petrologiya, Vol. 8, No. 2, 2000, pp. 199–224.

Late Archean Komatiites of the Ura Bay–Titovka Structure, Northwestern Kola Region

V. F. Smolkin*, V. V. Borisova*, S. A. Svetov, and A. E. Borisov***

** Geological Institute, Kola Research Center, Russian Academy of Sciences, ul. Fersmana 14, Apatity, Murmansk oblast, 184200 Russia*
e-mail: smolkin@geo.kolasc.net.ru

*** Geological Institute, Karelian Scientific Center, Russian Academy of Sciences, Pushkinskaya ul. 11, Petrozavodsk, 185610 Karelia, Russia*
e-mail: ssvetov@post.krc.karelia.ru

Received June 8, 1999

Abstract—The extended Northern Kola greenstone belt was formed within the Kola granulite–greenstone terrane in the Late Archean. Its lower part consists of volcanogenic basalt–komatiite sequences metamorphosed to amphibolite facies. The most representative and well preserved these rocks were found in the western part of the belt, in the middle reaches of the Ura, Western Litsa, and Titovka rivers. The rocks of the komatiite association compose massive and pillow lavas, differentiated lava flows, horizons and lenses of lava breccias and agglomerate tuffs of variable thickness and length, as well as subvolcanic bodies. The komatiites and basalts are products of areal subaqueous eruptions. Volcanic eruptions were accompanied by occasional phreatic explosions. The scarce differentiated flows consist of cumulate, spinifex-textured, and brecciated zones. Temperature and pressure in the mantle source are estimated as 1734°C and 7–8 GPa, respectively. The temperature of erupted lavas was about 1520°C. Geochemically, the komatiites approximate the Yilgarn type but show somewhat lower Al_2O_3/TiO_2 ratio. They experienced intense three-stage metamorphism. The first stage produced serpentine–magnetite and later chlorite–tremolite assemblages with partial preservation of primary magmatic high-Mg olivine. The second stage resulted in the local extensive development of olivine porphyroblasts owing to chlorite breakdown at 650–700°C. The third, retrograde stage caused the formation of carbonate and iddingsite–bowlingite. The intense carbonation was responsible for partial redistribution of REE and other elements.

INTRODUCTION

Since ultramafic volcanics have been first described near the Komati River, Barberton highland (South Africa) in the late 1960s (Viljonen, Viljonen, 1969), similar rocks termed komatiites were found on all Precambrian shields. Within the Baltic (Fennoscandian) shield, komatiites were studied in the Kuhmo Belt of Central Finland (Jahn *et al.*, 1980; Hanski, 1980), Karasjok belt of Norway (Often, 1985; Barnes and Often, 1990), Sumozero–Kenozero, Vedlozero–Segozero, and Gimola–Kostomuksha belts of Karelia (*Komatiity…*, 1988; *Zelenokamennye…*, 1988; *Metallogenicheskaya evolyutsiya…*, 1993; Svetov, 1997; Puchtel *et al.*, 1998). The Kola Region in the northeastern Baltic shield is relatively well studied, however komatiites were discovered there only in the late 1970s (Vrevsky, 1980). They were found in the western part of the Late Archean Kolmozero–Voron'ya structure, which resulted in the revision of its evolution scheme and ascribing to greenstone belts (*Zelenokamennye…*, 1988; Vrevsky, 1989; Smolkin *et al.*, 1991a, Smolkin, 1992). Therefore, the area Kolmozero Lake–Voron'ya River was considered as a test site for investigation of the structural features of greenstone belts within the Kola region, which is one of a few examples of granulite–greenstone terranes.

The western part of the Kolmozero–Voron'ya structure is characterized by the following features: (a) the development of a collisional suture between the large Murmansk and Central Kola geologic blocks (terranes) resulted in strong deformation of its internal structure and variable amphibolite-facies metamorphism; (b) the succession is represented by the lower terrigenous sequence changed upward by komatiite–basalt–jaspilite and basalt–andesite–dacite piles, which are unconformably overlain by the upper terrigenous sequence with komatiite pebble; (c) komatiites occur at two levels: interlayered with basalts (banded and sheared amphibolites), gneisses, and ferruginous quartzites in the lower part of the succession (above the lower terrigenous sequence) and associated with metabasalts and metagabbros in the upper part of the succession (below the upper terrigenous sequence); (d) komatiite bodies are structurally, mineralogically, and chemically heterogeneous and form a volcanoplutonic association, which consists of lava flows, sheeted and cutting dikes, and small plutons; and (e) typical differentiated flows with clear spinifex textures and (or) brecciated structures are very rare (Vrevsky, 1989; Smolkin *et al.*, 1991a; Smolkin, 1992).

To find representative komatiite outcrops, we revised various geological data, which showed that fragments of a greenstone belt may be found in the western extension of the collisional suture, in the middle reaches of the Ura, Western Litsa, and Titovka rivers. During field investigations of 1989 in the middle reaches of the Ura River, we discovered numerous outcrops of komatiitic volcanic rocks (Borisova *et al.*, 1991; Smolkin *et al.*, 1991b). Later, komatiites were also found in the basin of the Western Litsa and Titovka rivers (their middle and upper reaches) and in the watershed of the Titovka River–Pechenga Bay–Malaya Volokova Bay. This allowed us to distinguish the Ura Bay–Titovka structure, which we described together with the Kolmozero–Voron'ya structure as the Late Archean Northern Kola greenstone belt.

This paper presents results of the detailed geological and petrological investigations of the komatiite association of the Ura Bay–Titovka structure and discusses its genesis and metamorphism.

ANALYTICAL PROCEDURE

Field investigations of 1989–1990 and 1994–1995 included the search of outcrops of ultramafic bodies, study of their morphology and internal structure, and sampling for various kinds of analysis. In addition, we studied cores of prospecting boreholes, which recovered the Ambarnyi area, and the thin section collection of the Pechenga expedition. In 1998, we carried out additional short field investigations.

The samples were analyzed in the analytical laboratories of the Geological Institute of the Kola Research Center (Apatity), Geological Institute of the Karelian Research Center (Petrozavodsk), Institute of Precambrian Geology and Geochronology (St. Petersburg), Granada University (Spain), and Geological Survey of Finland (Otaniemi).

Minerals were analyzed on a Cameca MS-46 microprobe, analyst S.A. Rezhenova. Major and ore components were analyzed by the atomic absorption (Perkin Elmer 403 spectrometer) and XRF (VRA-33, VRA-31 spectrometers) methods. REE contents were determined by INAA in the Geological Survey of Finland and Institute of Precambrian Geology and Geochronology. Several samples were analyzed by ICP-MS using an MS Perkin Elmer Sciex elan 5000 spectrometer and Re, Rh, and In as internal standards following the technique of Parchett and Tatsumoto (1980). The measurement errors were 2 and 5% for elements with concentrations 100 and 10 ppm, respectively. The isotope investigations were carried out on a Finnigan MAT-261 mass-spectrometer in a static mode at the Institute of Precambrian Geology and Geochronology. Methods and main results of the isotope investigations were reported by Vrevsky *et al.* (1996).

GEOLOGY

The area under consideration represents a fragment of the Yarfjord–Kola Complex, which is part of the Servaranger–Kola terrane (Pozhilenko *et al.*, 1997, 1998). The terrane is distinctly separated from the Murmansk block (or terrane) by NE-trending faults, which are traced by geophysical methods to depths of about 35–40 km. The Servaranger–Kola terrane has a dome–block structure cut by Archean, Proterozoic, and Paleozoic faults. In the Early Proterozoic, the rocks were highly metamorphosed under amphibolite facies (Belyaev *et al.*, 1977; Belyaev and Petrov, 1991).

The Ura Bay–Titovka structure is traced discontinuously over 60 km from the middle reaches of the Ura River (40th km of the Murmansk–Zapolyarnyi highway) northwest to the upper reaches of the Titovka River. Its width is normally no more than 1–1.5 km and reaches 4 km in the vicinity of the Ura River. The eastern part of the structure is cut by relatively large polyphase subvolcanic plutons of the Svecofennian (1.81 Ga) porphyraceous granodiorites, granites, and monzonites of the Litsa–Ura Bay Complex. Its western continuation is represented by individual fragments of a greenstone belt among granite gneisses and migmatites. Similar fragments were observed on the northwest.

The basement of the zone consists of Late Archean amphibolite-facies rocks, which include para- and orthogneisses, amphibolites, magnetite schists, iron formation, and migmatites. These rocks were previously ascribed to the Kola Group and now are considered to belong to the unstratified Kola–Belomorian Complex (Radchenko *et al.*, 1994; Mitrofanov, 1996; *Kol'skaya sverkhglubokaya*, 1998). The gneiss–amphibolite complex is cut by Late Archean plutonic rocks (enderbites, charnockites, monzonites, tonalites, migmatites, and granite gneisses). In northern Norway, one of the high-temperature metamorphic stages was dated at 2719 ± 3 Ma by the U–Pb method. The plutons of quartz monzonites and hypersthene granites have similar ages: 2727 ± 24 Ma and 2706 ± 3 Ma, respectively (Levchenkov *et al.*, 1995). Tonalitic gneisses recovered by the Kola Superdeep Borehole show older U–Pb ages of 2835–2832 Ma (*Kol'skaya sverkhglubokaya*, 1998).

The Murmansk Block (terrane) consists predominantly of tonalitic gneisses, plagiogranites (or oligoclase granites), and migmatites with distinct zonation near the Titovka River: southward, amphibolite assemblages are replaced by biotite ones. Vetrin (1984) believes that this is related to a decrease in erosion level.

A relatively complete section of the Ura Bay–Titovka structure was observed in the middle reaches of the Ura River, 8–12 km from road fork of Murmansk–Zapolyarnyi to Ura Bay (Fig. 1). The southern part of this area consists predominantly of the NW-striking biotite and two-mica gneisses with interbeds of garnet–biotite gneisses, amphibole schists, and amphibolites. The gneisses and amphibolites are cut by thin subcon-

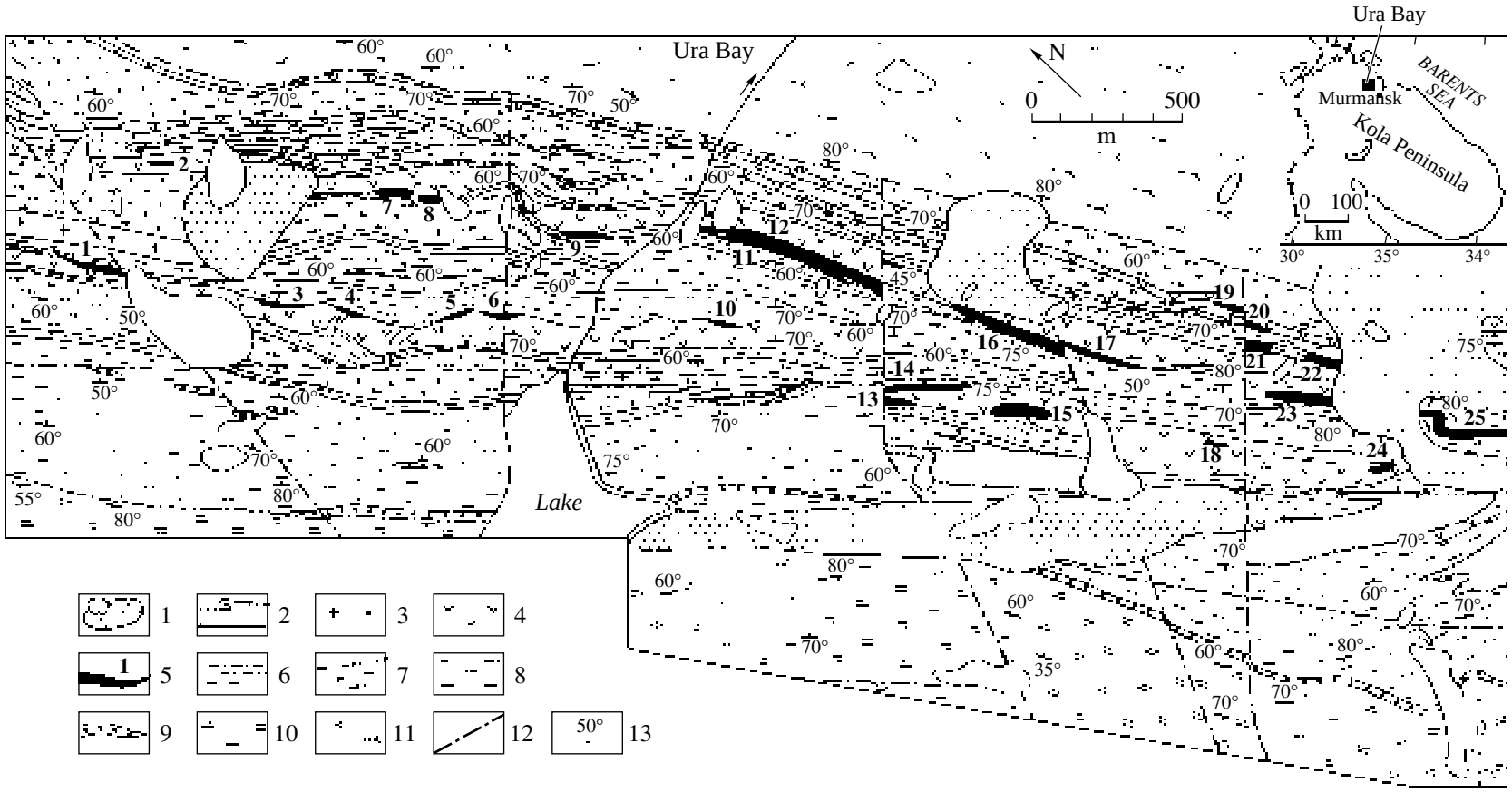

Fig. 1. Schematic geological map of the eastern part of the Ura Bay–Titovka structure, the Ura River. The map was constructed using data from prospecting work with our modifications.

(1) Lacustrine, bog, and moraine deposits; (2) large pegmatite vein; (3) microcline–plagioclase granite; (4) amphibolite, sheared amphibolite; (5) komatiite bodies including volcanic flows, sills, and agglomerate tuffs; body numbers; (6) high-Al (garnet–biotite, sillimanite–staurolite–biotite, kyanite–sillimanite–biotite, and biotite–andalusite) gneiss; (7) fine-grained biotite gneiss and plagiogneiss; (8) medium-grained biotite gneiss and two-mica tourmaline-bearing gneiss, swarm of thin pegmatitic veins; (9) conglomerate and gravelstone; (10) biotite, garnet–biotite, and two-mica gneiss of the basement and plagiomicrocline granite cutting it; (11) tonalite, plagiogranite, migmatite, and crosscutting plagiomicrocline granite of the Murmansk block; (12) fault; (13) strike and dip of gneissosity and shearing.

cordant bodies of the plagiomicrocline gneissic granites and bodies of granite pegmatites with quartz–muscovite mineralization. The gneisses and amphibolites are overlain by conglomerates and presumably represent basement rocks.

The generalized section of this structure is divided into three sequences: lower terrigenous with conglomerates, middle volcanogenic komatiite–basalt, and upper volcanogenic–sedimentary composed of various gneisses and more rare amphibolites.

The metamorphosed pebble, occasionally rubble–pebble conglomerates occur in the base of the lower terrigenous sequence as a distinct nearly continuous basal horizon (Fig. 1). Its thickness ranges from 2 to 5 m, occasionally up to 10 m. This horizon rests on migmatized gneisses and plagiogranites and contains their pebbles. The pebbles range from 3×5 to 5×10 cm in size and account for no more than 30–35% of the total metaconglomerate volume. Thin lenses of pebble conglomerates also occur throughout the whole terrigenous sequence. In spite of the development of gneissic structures, the basal horizon and upper lenses show a distinct graded bedding.

The lower terrigenous sequence consists predominantly of medium-grained biotite, two-mica, and tourmaline-bearing gneisses. Relicts of thin bedding and gravel–sandy textures suggest their terrigenous origin. The sequence contains abundant NW-trending subconcordant lenticular bodies of tourmaline-bearing pegmatites. Their thickness ranges mainly within several meters, but occasional platelike bodies are up to 130–150 m thick.

The contacts and gneissosity within the middle volcanogenic sequence (500–650 m in thickness) dip steeply northeast, occasionally northwest (60°–70°). This sequence consists of metamorphosed komatiites and basalts (amphibolites) with horizons of various gneisses and plagiogneisses. The latter are mainly represented by fine-grained biotite gneisses with subordinate thin layers and lenses of garnet–biotite, sillimanite–staurolite–biotite, kyanite–sillimanite–biotite, and biotite–andalusite gneisses. The sequence is cut by veins of tourmaline-bearing granite pegmatites and platelike bodies of microcline–plagioclase tourmaline–muscovite granites, up to 75 m thick. The granites are subconcordant or cross-cutting, they show gneissic structures and form apophyses. The tourmaline-bearing pegmatites of the area host low-grade rare-metal mineralization (accessory beryl and columbite) (Gordienko and Charikov, 1998).

Komatiites and basalts associate spatially and interlay in the sequences. Two distinct komatiite levels with different morphologies and structures of komatiite bodies can be recognized. In spite of intense shearing and metamorphism, the komatiites show occasionally evidence of volcanogenic origin, which is described below. Basalts are represented by amphibolite bodies from 10–20 to 100–130 m thick. The thickness does not vary significantly along the strike. They show uniform, banded, and sheared varieties, which may intercalate in the section forming units. Judging from the relict amygdaloidal and pillowed structures, such an alternation could be formed during repeated eruptions of volcanic flows and tuffs. The apparent thickness of individual flows is 3–5 m. The amphibolites normally show medium-grained, nematoblastic, occasionally relict gabbroic or gabbro-ophitic textures. Some amphibolites presumably represent subvolcanic gabbroids. Local migmatization considerably transforms the amphibolites and increases their heterogeneity.

The upper volcanogenic–sedimentary sequence consists mainly of fine-grained biotite gneisses with scarce thin amphibolite and sheared amphibolite bodies, as well as with individual lens-shaped beds of high-Al gneisses. At the north, they are separated from the Murmansk Block (terrane) by a complex steep fault system. Most of the gneisses correspond compositionally to dacites and rhyolites, and paragneisses with relicts of sedimentary bedded structures occur in minor amount.

All the rocks experienced intense textural and tectonic transformations (shearing, isoclinal folding) and high-temperature metamorphism. The mineral assemblages and reconstruction of *P–T* parameters indicate amphibolite andalusite–sillimanite and kyanite–sillimanite metamorphism (Belyaev *et al.*, 1977; Belyaev and Petrov, 1991).

As compared to the western part of the Kolmozero–Voron'ya structure (Vrevsky, 1985; Smolkin *et al.*, 1991a), the Ura Bay–Titovka structure is characterized by considerably lower thicknesses of the generalized section and individual sequences; absence of iron formation, upper terrigenous sequence, and upper komatiite level; and preservation of total succession of rock associations from terrigenous rocks to mafic–ultramafic and acid volcanics.

KOMATIITE FACIES

Various lava flows, lens-shaped horizons of lava breccias and agglomerate tuffs, and sills occur in the northeastern part of the structure, in the middle reaches of the Ura River. Various facies show regular spatial distribution: the lower level contains mainly lava flows (Fig. 1, bodies 3–6, 10, 13–15, 18, 24) and subordinate sills (1), whereas the upper level consists predominantly of sills (7–9, 12, 16–17) with subordinate amount of lavas (2, 11, 19–23, 25) and agglomerate tuffs (near 11, 15).

The lava flows are 3–5 to 10–20 m thick and 100–250, occasionally up to 500 m long. In some places, the flows intercalate with lava breccias and agglomerate tuffs, forming units up to 100 m thick.

The volcanic rocks are divided into massive, pillow, and brecciated lavas and differentiated lava flows with brecciated and olivine spinifex-textured zones (Fig. 2).

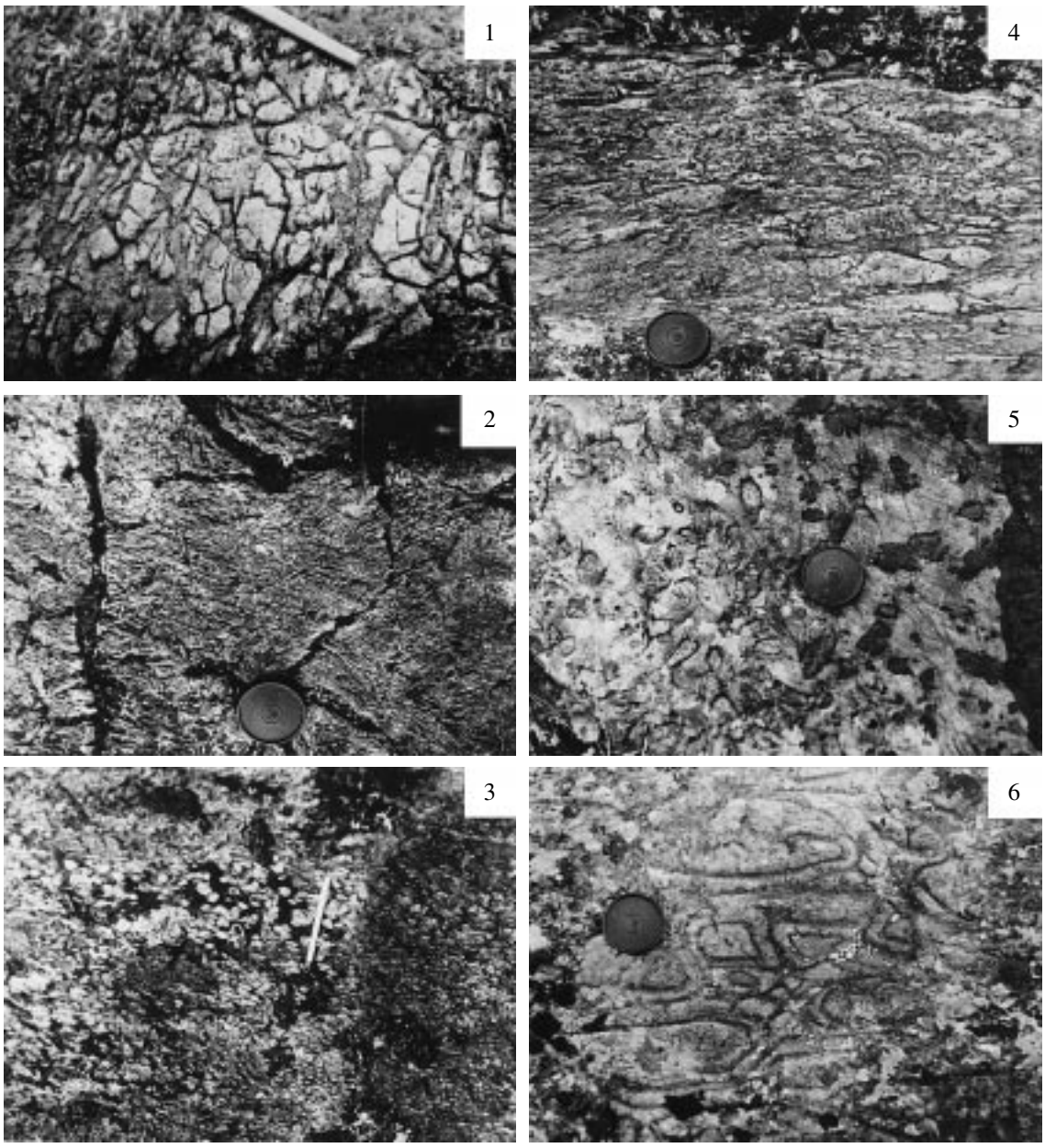

Fig. 2. Textural and structural features of komatiites (outcrop photos).
(1–3) Differentiated flow (Fig. 1, no. 6): (1) brecciated zone, (2) olivine pocket–plated spinifex, and (3) olivine–cumulative zone; (4) agglomerate tuff (Fig. 1, no. 15), (5) porphyroblastic komatiite, Western Litsa River; (6) pillow lava.

The massive lavas are relatively uniform, whereas the pillow lavas exhibit vague pillow and ball structure. Unlike the "balls," "pillows" are flattened and vary from 30 to 80 cm in length and from 20 to 30 cm in width (Fig. 2). The balls and pillows account for 60–70% of the total lava volume. The least sheared balls occasionally show primary radiating and concentrical fissures. The brecciated lavas consist of highly fractured irregular small fragments (several centimeters across) and a relatively homogeneous lava cement. The fragments and cement are composed of carbonate–amphibole–chlorite aggregate with minor magnetite and ilmenite.

In spite of the low abundance (Fig. 1, nos. 5, 6, 11, 15), the differentiated lavas are very important for komatiite diagnostics. The least altered differentiated flow (9 m thick) was observed at the contact between amphibolites and overlying gneisses, north of the road toward the Ura Bay (no. 6). The flow is divided into the lower cumulate (4.0–5.0 m), middle spinifex (3.5–4.0 m), and upper brecciated (1.0–1.5 m) zones, which are separated by sheared contacts (Fig. 3a). The cumulate zone

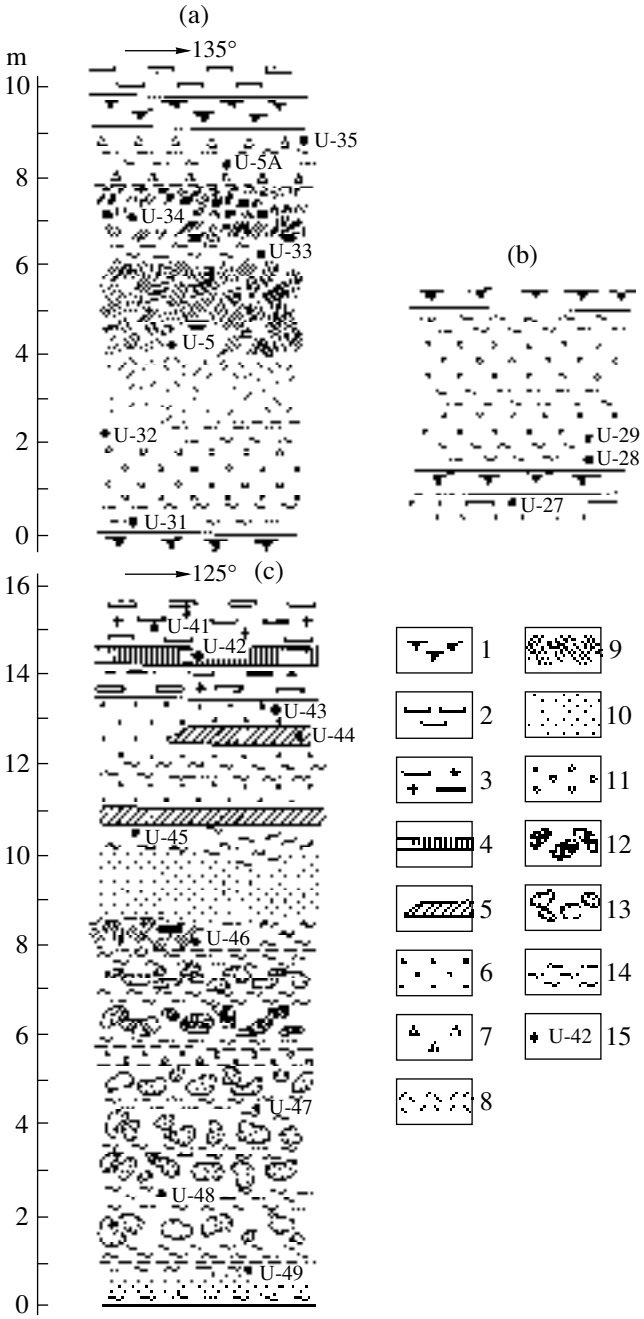

Fig. 3. Schematic geological sections of a differentiated lava flow, Ura River.

(1) Quaternary deposits; (2) garnet–biotite gneiss; (3) garnet–biotite gneiss cut across by quartz–feldspar veinlets; (4) plagioamphibolite; (5) amphibolite; (6) pyroxenite komatiite; (7) flowtop komatiite breccia; (8) scattered olivine spinifex; (9) pocket–plated olivine spinifex; (10) massive fine-grained komatiite; (11) medium-grained porphyritic komatiite, including that from the cumulate zone; (12–13) brecciated lava with komatiite fragments with (12) microspinifex and (13) fine-grained textures; (14) shearing; and (15) location and number of sample.

consists mainly of chlorite–carbonate–tremolite aggregate with scarce serpentine pseudomorphs after olivine. The grain size decreases toward the thin sheared lower chilled margin. Toward the top of the spinifex zone, scattered coarse-plated spinifex changes to fine-plated and pocket spinifex. The plates within pockets are often bent. They are up to 10 cm long at 1–1.5 mm thick. The plated and pocket–plated aggregates are replaced by fine flaky chlorite, which is embedded in a tremolite–cummingtonite–chlorite groundmass with minor carbonate, magnetite, and ilmenite. No relicts of primary olivine were found, but the morphology of pseudomorphs is fairly similar to that described in slightly altered komatiites from Canada, South Africa, and south India (*Komatiites*, 1982). They contain plated–skeletal olivine and skeletal pyroxene in the groundmass.

The upper brecciated zone contains irregular flattened fine-grained fragments, of 3–5 by 5–10 cm in size and a fine-grained cement. The fragments and cement are characterized by similar mineral compositions (carbonate, chlorite, and amphibole), but differ in color because of various proportions of these minerals. Morphologically, these rocks resemble brecciated lavas, but differ in somewhat lower abundance of fragments. Along the strike, the layering of the lavas may become less distinctive (Fig. 3b).

Complex sequences, which were presumably formed during repeated lava filling of the lowlands (small depressions and trenches) occur occasionally. The total apparent thickness of one such sequence is more than 13 m (Fig. 3c). From bottom to top, it consists of massive lava, several microflows of brecciated lava, massive lava, and interlayered sheared lavas of peridotite and pyroxenite komatiites and basalts. The brecciated lavas contain 3–10 cm fragments with aphyric, fine porphyritic, or microspinifex textures. The bent shape of the spinifex aggregates suggests that the fragments experienced plastic deformations during viscous lava flow. This sequence records no less than five komatiite eruptions. They were presumably separated by small time gaps, which were not large enough to the previous melt portion has crystallized completely. Based on these data, this sequence may be ascribed to lava "paleolakes."

The agglomerate tuffs (Fig. 1, nos. 11a, 15) consist of flattened or irregular rounded fragments, which are cemented by a fine-grained tuffaceous carbonate–chlorite–amphibole groundmass with vague bedding (Fig. 4). The fragments range from 1–10 to 15–20 cm in size and from 70–80 to 40–50% in abundance. However, the sizes and abundance of fragments relatively slightly varies within individual outcrops and graded bedding is poorly expressed.

The subvolcanic komatiite bodies (sills) are thick (20–50 m) and long (200–1000 m and more) and show no distinct layering (Fig. 4). Because the contacts are normally strongly sheared, chilled zones are not preserved. Most of such bodies consist of serpentine–chlo-

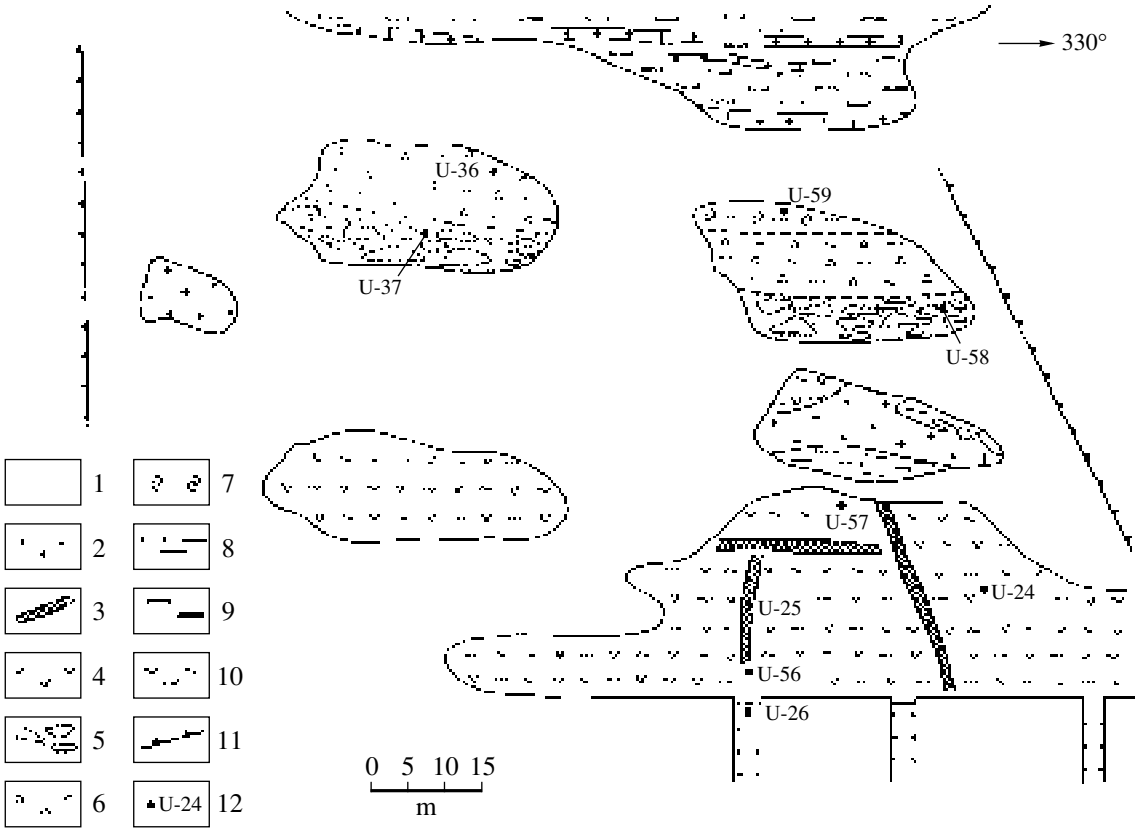

Fig. 4. Schematic geological plan of the distribution of agglomerate tuffs and sills, Ura River area.
(1) Quaternary deposits; (2) granite pegmatite; (3) serpentine–asbestos veinlet; (4) komatiite; (5) agglomerate komatiite tuff; (6) brecciated lava; (7) pillow lava; (8) amphibolite; (9) garnet–biotite gneiss; (10) shearing; (11) rocky scarp; and (12) location and number of sample.

rite–amphibole rocks with minor carbonate, talc, magnetite, and ilmenite. Chlorite–serpentinite and chlorite–tremolite schists are less common. The subvolcanic bodies contain complex networks of fibrous serpentine–asbestos veinlets.

The Ura Bay–Titovka structure is characterized by the presence of komatiites with large porphyroblasts of secondary olivine (Borisova *et al.*, 1998). Such rocks occur occasionally in the middle reaches of the Ura River (Fig. 1, southwestern part of body no. 11) and are abundant in the watershed of the Western Titovka–Litsa rivers. The irregular distribution of prophyroblasts in the groundmass results in the spotted structure of the rock (Fig. 2). Porphyroblasts are common in the relatively uniform massive or pillow lava flows, and also develop in individual sheared zones.

Only individual fragments of greenstone belts are preserved in the middle reaches of the Western Litsa and Titovka, and within their watershed. These fragments consist of massive, pillow, and brecciated komatiite lavas and strongly sheared porphyroblastic rocks. Porphyroblastic komatiites compose up to 50% of the total sequence with an apparent thickness of 200–250 m. A study of drill cores showed that the komatiites associate often with amphibolites and dip steeply to the southwest. In addition to volcanic rocks, steeply dipping serpentine–amphibole–chlorite lenses occur. As seen in the core, these lenses have no primary layering.

MINERAL COMPOSITION

Because of metamorphism, the primary mineral assemblage preserved only as individual small relicts in the komatiites, which prevents deciphering crystallization processes.

Judging from pseudomorphs, magmatic olivine crystallized as morphologically diverse grains and intergrowths. In the cumulate zones of the differentiated flows and subvolcanic bodies it formed small (0.3–2.0 mm) equant columnar phenocrysts or glomerophyric intergrowths, which are replaced by aggregate of reticulate serpentine with sectorial extinction and disseminated magnetite. Individual pseudomorphs contain small (0.1 mm) relicts of irregular olivine, which are cut by serpentine veinlets. Spinifex zones contain individual plated skeletal crystals or pockets of plated crystals of various orientation, which are completely altered

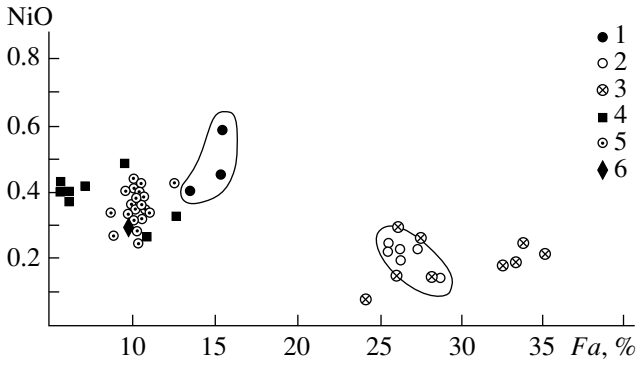

Fig. 5. NiO–*Fa* diagram for magmatic and metamorphic olivine from the komatiites of the Ura Bay–Titovka structure and other areas.

(1) Relict olivines from the cumulate zone of the differentiated pillow flow and sill, Ura River; (2) porphyroblastic olivine from komatiites, Western Litsa River; (3) metamorphic olivine from Finland picrites (Peltonen, 1990); (4) magmatic olivine from Alexo and Munro Township komatiite flows, Canada (Barnes *et al.*, 1983; Arndt, 1986); (5) olivine from lherzolite nodules in volcanics (Shcheka, 1983); (6) olivine in peridotite xenolith from the breccia pipes of the Khibina Massif, Kola Peninsula (Arzamastsev *et al.*, 1988).

to chlorite–amphibole aggregate with subordinate magnetite.

The relict olivine from the serpentine pseudomorphs was analyzed in polished thin sections and mineral separates. Compositionally, it corresponds to chrysolite with small variations of fayalite mole fraction (13.5–15.5%) (Table 1). Olivine from the volcanic rocks has higher Fe content than olivine from the sills.

Olivine from the slightly altered Archean komatiites of the Munro Township and Alexo (Canada) demonstrates higher compositional variations throughout the sequence of differentiated flows and contains 6–11% *Fa* in the cumulate and brecciated zones and 9–15% *Fa* in the spinifex zone (Arndt, 1977, 1986; Barnes *et al.*, 1983). The earliest olivine (from the cumulate zone) is the most magnesian. The relict olivine from the Ura Bay komatiites is higher in fayalite mole fraction than olivines from Canadian komatiites, as well as from nodules and mantle xenoliths (Fig. 5). Therefore, we suggest that the analyzed olivine is relatively late.

The relict olivine from the Ura Bay is characterized by very low CaO content (less than 0.04 wt %), in contrast to olivine from Canadian komatiites (from 0.12% to 0.30 wt % CaO). According to Simkin and Smith (1970), plutonic and volcanic rocks are discriminated at 0.1 wt % CaO in olivine. However, there are many exceptions. In particular, CaO content (0.13–0.36 wt %) in olivine–chrysolite from the Pechenga Ni-bearing peridotites is similar to that in olivine from the comagmatic ferropicritic flows (Smolkin and Pakhomovskii, 1985; Smolkin, 1992). Experiments on low-pressure komatiite crystallization revealed that CaO content in olivine depends on temperature. It was less than 0.01 wt % at 1300°C and increased to 0.15 wt % at 1200°C (Smolkin, 1992). However, Ca could be removed from olivine during metamorphism. This problem is poorly studied and requires additional investigations.

Olivines from the Archean komatiites show higher Ni content (from 0.37 to 0.55 wt %) than those from mafic volcanics (Fig. 5). In particular, relict olivine from the Ura Bay contains 0.40–0.58 wt % NiO (at higher Fe content). It is known that Ni content in silicate mafic melts decreases rapidly during the crystallization of early magnesian olivine; thus providing lower NiO content of later Fe richer olivines. However, in the presence of sulfur, NiO content in olivine increases with increasing content of the sulfide phase (Arutyunyan *et al.*, 1988); i.e., sulfide serves as a buffer. Therefore, the primary silicate melt could contain a sulfide phase.

Primary pyroxenes (clinopyroxene and more rare orthopyroxene) occur as small (1.0–2.0 mm) relicts

Table 1. Chemical composition of magmatic and metamorphic olivine from the komatiite rock association of the Ura Bay–Titovka structure, wt %

Component	U-5b	U-59	U-40	U-60	U-60a	U-24	WL-1a	WL-1b	WL-1c
SiO_2	39.07	39.24	39.25	38.74	40.50	35.88	37.94	38.21	37.80
FeO*	14.61	14.80	13.14	23.26	23.86	24.18	24.74	23.24	23.21
MnO	0.08	0.25	0.16	0.53	0.51	0.37	0.34	0.52	0.44
MgO	44.79	45.52	47.48	37.00	33.41	38.65	37.11	38.26	38.20
CaO	0.00	0.04	0.04	0.04	0.03	0.00	0.00	0.00	0.00
NiO	0.58	0.45	0.40	0.19	0.14	0.22	0.22	0.22	0.24
Total	99.13	100.30	100.47	99.76	98.48	99.30	100.35	100.45	99.89
Fa, %	15.5	15.4	13.5	26.1	28.6	25.9	27.21	25.4	25.4

Note: Relicts of primary olivine from the cumulate zone of the differentiated flow (U-5b), pillow lava (U-59), and sill (U-40); porphyroblastic olivine from flows (U-60, WL-1) and sill (U-24). (U) Ura River, (WL) Western Litsa River. FeO* = FeO + Fe_2O_3. Analyses were performed on a Cameca MS-46 microprobe, analyst S.A. Rezhenova.

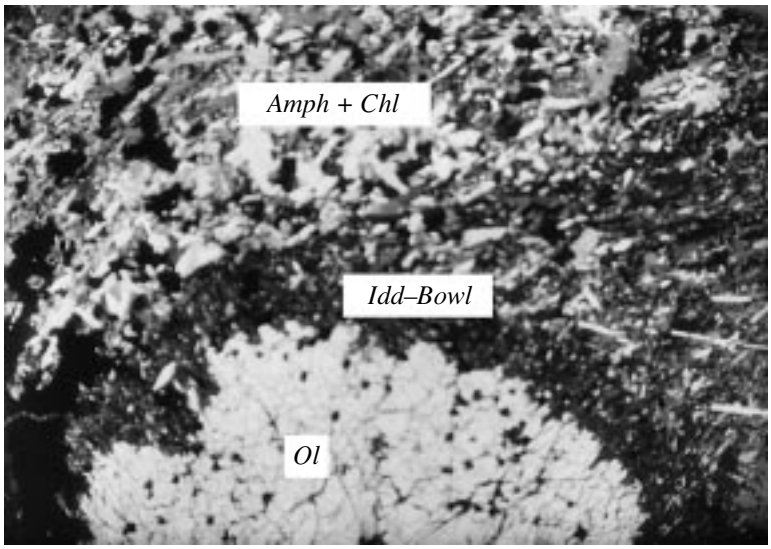

Fig. 6. Porphyroblastic olivine (*Ol*) with iddingsite–bowlingite rim (*Idd–Bowl*) in the amphibole–chlorite (*Amph + Chl*) groundmass (Western Litsa River). Thin section, polarized light.

within amphibole pseudomorphs after porphyritic phenocrysts only in the subvolcanic bodies.

The Precambrian komatiites contain primary Al-rich chrome spinel, which is stable under a wide range of *P–T* parameters (from greenschists to amphibolite facies) (Plaksenko and Smolkin, 1990; Zhou and Kerrich, 1992). However, the komatiites studied, instead of primary chrome spinel, contain secondary Cr-bearing magnetite. Cr could be derived from both chrome spinel (more likely) and mafic minerals such as olivine and pyroxene.

The metamorphic assemblage of the volcanogenic komatiites is represented mainly by amphibole, chlorite, and carbonate. The mineral proportions are as follows (vol %): 55–85 tremolite–actinolite, 10–30 chlorite, and from 2–3 to 15 carbonate. The subvolcanic bodies consist mainly of serpentine–chlorite–amphibole, occasionally chlorite–serpentine assemblages with strong serpentine predominance (to 85%). Serpenite is represented by fine-grained, occasionally acicular–fibrous antigorite. In some cases, the amphibole aggregates are cut by serpentine veinlets. In addition to tremolite–actinolite, scarce acicular–prismatic anthophyllite and cummingtonite were found. Carbonate occurs as small porphyroblastic grains and (or) composes thin veinlets cutting the fine-grained groundmass.

As was mentioned above, the komatiites of the Ura Bay–Titovka structure are characterized by the occurrence of large porphyroblasts of secondary olivine. They have lenticular or irregular–rounded shape, dark brown color, and are separated by distinct light gray rims from the green groundmass. The porphyroblasts range from 0.1 to 6–8 cm in size, mainly 1–2 cm, and account for a few to 60–70% of the total volume at very irregular distribution. A rock with such porphyroblasts normally does not contain relicts of primary olivine.

Microscopically, porphyroblasts consist of a single large olivine crystal (Fig. 6) or aggregate of grains with variable extinction, which form the glomeroporphyroblastic texture. The porphyroblasts contain numerous inclusions of aggregates of tremolite, chlorite, and magnetite, which are major constituents of the groundmass. They do not show the stringer–reticulate texture which is typical of serpentine. The rims of porphyroblast, 1–5 mm thick, consist of reddish (in thin sections) iddingsite, greenish–yellow bowlingite, or often a mixture of these two minerals. The rims also contain numerous inclusions of groundmass minerals.

Microprobe investigations showed relatively narrow variations of *Fa* content in the individual grains and aggregates of secondary olivine (25.4–28.6%) (Table 1), which is higher than Fe/(Fe + Mg) ratio of the host rock (f = 17.4–18.6%). Secondary olivine also has higher MnO (0.34–0.53 wt %) and lower NiO content (0.14–0.24 wt %) than the relicts of primary olivine.

The metamorphic association of secondary olivine includes low-Fe tremolite–actinolite, chlorite, relatively high-Fe bowlingite, and magnetite with significant Cr, Al, Ni, Zn, and V contents (Table 2). Tremolite and actinolite from the groundmass and microinclusions are compositionally similar.

The highest Fe porphyroblastic olivines are clustered in a compact field at the right part of the *Fa*–NiO diagram (Fig. 5). Their composition is not correlated with that of the host rock. As seen in Fig. 5, their field is overlapped by morphologically similar secondary olivines from the metamorphosed Svecofennian picrites of southern Finland (Peltonen, 1990), which indicates their metamorphic genesis.

Table 2. Chemical compositions of metamorphic minerals from inclusions in olivine porphyroblasts and groundmass, wt %

Component	$Trem_1$	Chl_1	Mgt_1	$Trem_2$	Chl_2	Mgt_2	*Bowl*
SiO_2	52.05	28.77	0.00	55.50	29.66	0.00	40.13
TiO_2	0.21	0.08	0.74	0.11	0.08	0.92	0.02
Al_2O_3	4.60	18.08	0.08	2.54	17.13	0.14	0.00
FeO*	5.56	7.39	87.88	5.21	8.48	87.00	20.82
MnO	0.18	0.02	0.14	0.18	0.05	0.16	0.52
MgO	20.71	31.15	0.16	22.30	30.57	0.16	23.67
CaO	11.93	0.00	0.00	11.22	0.03	0.00	0.27
Na_2O	0.84	0.06	0.00	0.60	0.00	0.00	–
K_2O	0.08	0.00	0.00	0.04	0.02	0.00	0.04
Cr_2O_3	0.12	0.33	4.19	0.01	0.49	5.34	–
NiO	0.08	0.15	0.16	0.06	0.14	0.19	0.01
Total	99.36	85.96	93.77	97.77	86.64	94.41	85.48
f, at.%	13.2	11.8	–	11.5	13.5	–	33.0

Note: (WL-1) porphyroblastic komatiite, Western Litsa River. ($Trem_1$) tremolite, (Chl_1) chlorite and (Mgt_1) magnetite from the groundmass; ($Trem_2$) tremolite, (Chl_2) chlorite, and (Mgt_2) magnetite from inclusions in olivine porphyroblasts; (*Bowl*) bowlingite from the porphyroblast rim. Mgt_1 also contains 0.40% V_2O_5 and 0.02% ZnO; Mgt_2 contains 0.48% V_2O_5 and 0.02% ZnO. FeO* = FeO + Fe_2O_3, *f*, at. % = 100Fe*/(Fe* + Mg). Analyses were performed on a Cameca MS-46, analyst S.A. Rezhenova.

CHEMICAL AND ISOTOPE COMPOSITION OF KOMATIITES AND BASALTS

Komatiites from the structure studied are high-Mg rocks with high Cr and Ni and low TiO_2, Na_2O, K_2O, and P_2O_5 (Tables 3, 4).

The 100Fe/(Fe + Mg) atomic ratio (*f*) ranges generally between 13.0 and 24.0: within 13.0–16.4 in the pillow lavas; 16.0–24.0, in the differentiated lava flows; 18.0–21.0, in the massive lavas, lava breccias, and agglomerate tuffs; and 14.7–21.0, in sills. The porphyroblastic komatiites show the same *f* values (17.4–18.3). The komatiites with low MgO content (13–16 wt %) show higher *f* values (to 29.6–35.5). The basalts (amphibolites) are characterized by the highest *f* (39.8–55.1) and TiO_2 content (0.7–1.1 wt %).

Cr and Ni are the most important ore components in Archean komatiites. Their contents range within 1780–3010 and 1100–2100 ppm, respectively, in lavas, and within 1780–2950 and 1100–2280 ppm, respectively, in the subvolcanic bodies. The komatiites with low MgO content are lower in Cr (to 1500 ppm) and Ni (to 440 ppm). The basalts are lowest in Cr (70–340 ppm) and Ni (70–200 ppm) at slightly higher V content (110–280 ppm). Sulfur in all the komatiites studied is related to fine dissemination of pyrrhotite.

To typify the komatiites, we used the classification diagrams Al_2O_3–(FeO*)/(FeO* + MgO), CaO–MgO–Al_2O_3, and Al_2O_3–(FeO* + TiO_2)–MgO (Fig. 7). These diagrams show that the rocks do not form a continuous series, but are clustered in three separate fields. Field I includes data points of the komatiite lava flows, tuffs, and subvolcanic bodies. Field II includes lower MgO rocks (13–16 wt %) from scarce thin bodies. Field III includes amphibolites that correspond chemically to Fe tholeiites or tholeiitic basalts with the lowest MgO content (6–10 wt %). In these diagrams, the compositions of the volcanogenic and subvolcanic rocks overlap considerably, while the sills show relatively slight variations in major components.

The line MgO/(MgO + Al_2O_3 + FeO + TiO_2) = 0.6 (Fig. 7c) divides the komatiites studied into two fields, corresponding to peridotite and basaltic komatiites according to the classification proposed Viljonen and Viljonen (1969) and accepted at the Penrose conference (Komatiites, 1982). We believe that such a division is formal, because mineralogically and chemically similar rocks from a single body may be ascribed to different rock types. More reasonable is the classification of Arndt *et al.* (1977), which distinguishes peridotite (MgO > 20 wt %), pyroxenite (MgO = 12–20 wt %), and basalt (MgO < 12 wt %) komatiites. According to this classification, transitional rocks should be ascribed to pyroxenite komatiites. Therefore, we distinguished peridotite and pyroxenite komatiites, and Fe tholeiite within the structure. The nearly complete absence of transitional rocks between komatiites and basalts suggests that they are not genetically related.

Two principal types of komatiites have been distinguished on the basis of their chemical composition: (1) less abundant Al-depleted or Barberton-type komatiites with CaO/Al_2O_3 = 1.5, Al_2O_3/TiO_2 = 10, $(La/Sm)_N$ = 1, and $(Gd/Yb)_N$ = 1.4; and (2) more common Al-undepleted or Yilgarn-type komatiites with CaO/Al_2O_3 = 1.0, Al_2O_3/TiO_2 = 21–25, $(La/Sm)_N$ = 0.4–0.8, and $(Gd/Yb)_N$ = 1.05 (Nesbitt *et al.*, 1982). In the diagram CaO–MgO–Al_2O_3 (Fig. 7b), most of the data points of

Table 3. Chemical composition of komatiites from lava flows and horizons of agglomerate tuffs and host amphibolites (basalts) of the Ura Bay–Titovka structure (major elements in wt%, trace elements in ppm)

Component	LMZ	CZ		SpZ			BZ		PxK	A(B)	CZ		ML
	U-5b	U-31	U-32	U-5	U-33	U-34	U-5a	U-35	U-4	U-27	U-28	U-29	U-49
SiO_2	41.75	37.28	35.15	41.44	41.44	38.96	42.45	41.55	47.75	49.91	45.03	40.00	40.53
TiO_2	0.52	0.36	0.37	0.39	0.36	0.46	0.44	0.55	1.01	1.02	0.31	0.30	0.46
Al_2O_3	5.58	4.85	4.18	5.49	6.08	6.70	6.66	8.43	8.86	13.44	5.85	5.36	6.10
Fe_2O_3	7.46	3.17	1.66	3.94	2.11	3.87	4.79	3.72	3.38	4.74	5.59	3.44	4.98
FeO	5.75	6.66	6.98	7.21	7.61	7.45	6.48	6.39	8.61	9.05	4.52	5.94	6.76
MnO	0.14	0.14	0.15	0.09	0.12	0.11	0.14	0.12	0.21	0.18	0.13	0.17	0.13
MgO	22.25	25.93	27.01	27.68	26.96	26.85	25.30	25.53	13.97	7.07	23.96	26.67	25.53
CaO	8.59	5.67	6.94	2.28	2.97	2.54	4.86	4.23	12.82	8.01	6.73	4.62	4.26
Na_2O	0.07	0.02	0.02	0.02	0.02	0.02	0.04	0.06	1.11	4.35	0.11	0.02	0.04
K_2O	0.01	0.01	0.01	0.01	0.01	0.01	0.01	0.02	0.15	0.15	0.01	0.01	0.01
H_2O^-	0.01	0.37	0.36	0.28	0.46	0.61	0.16	0.44	0.06	0.29	0.48	0.60	0.39
LOI	5.67	6.18	5.89	6.84	7.05	7.72	6.31	7.79	1.92	1.74	6.40	6.79	6.75
P_2O_5	0.04	0.03	0.04	0.04	0.05	0.02	0.07	0.04	0.07	0.08	0.01	0.02	0.06
CO_2	1.97	8.16	10.49	3.58	4.11	3.63	1.82	0.17	0.11	0.10	0.57	5.93	3.07
S_{tot}	0.00	0.21	0.13	0.12	0.10	0.16	0.27	0.05	0.00	0.01	0.07	0.06	0.05
Cr	3010	2390	2190	2460	2260	2800	2390	2740	1500	70	2190	2190	2670
V	170	160	120	110	130	160	170	170	220	280	110	110	150
Ni	1100	1800	1700	1100	1400	1400	1500	1100	440	120	1400	1500	1800
Co	140	110	110	80	100	120	140	110	100	80	120	120	110
Cu	10	150	80	58	60	90	100	30	10	70	70	40	150
f, at. %	24.0	17.0	15.0	17.7	16.5	18.6	19.3	17.6	31.9	51.0	18.0	16.0	20.0
No.	6									6			

Component	LB		SpZ	SK	A(B)	ML	A(B)	PilL		LB	SK	SK	PxK
	U-48	U-47	U-46	U-45	U-44	U-43	U-42	130	131	133	134	135	136
SiO_2	43.72	46.37	47.41	46.57	47.62	47.05	53.83	47.52	47.76	50.06	44.19	47.33	48.06
TiO_2	0.38	0.31	0.34	0.32	0.98	0.43	0.70	0.38	0.33	0.32	0.57	0.37	0.65
Al_2O_3	6.28	5.29	4.70	5.57	13.89	6.85	13.45	7.44	6.47	5.54	9.40	6.03	10.82
Fe_2O_3	5.22	3.25	3.08	2.47	2.39	2.43	2.85	1.94	2.39	1.17	3.81	4.89	2.32
FeO	5.72	7.65	7.42	8.09	10.47	7.24	6.90	7.27	7.65	8.06	8.04	6.55	10.07
MnO	0.11	0.15	0.15	0.18	0.18	0.15	0.15	0.15	0.16	0.14	0.14	0.17	0.22
MgO	24.56	26.55	25.50	22.70	8.68	20.50	7.47	27.52	28.09	30.03	28.22	28.46	16.25
CaO	5.48	2.28	3.46	6.10	10.47	7.93	8.28	7.39	6.76	4.39	5.30	6.02	10.11
Na_2O	0.08	0.04	0.05	0.14	2.81	0.44	3.19	0.29	0.27	0.22	0.22	0.12	1.30
K_2O	0.01	0.01	0.02	0.02	0.17	0.07	0.33	0.02	0.04	0.02	0.02	0.01	0.10
H_2O^-	0.47	0.43	0.43	0.44	0.26	0.47	0.31	0.21	0.40	0.21	0.41	0.31	0.11
LOI	6.88	6.45	6.25	6.03	2.23	5.41	1.85	7.33	8.80	8.30	8.02	6.98	1.84
P_2O_5	0.02	0.01	0.04	0.01	0.06	0.04	0.35	0.08	0.07	0.04	0.08	0.07	0.09
CO_2	0.02	0.32	0.14	0.23	0.15	0.08	0.07						
S_{tot}	0.04	0.10	0.18	0.20	0.01	0.00	0.02						
Cr	2670	2190	2120	2190	390	270	340						
V	180	110	110	110	110	110	280						
Ni	1200	1500	1500	1100	200	800	70						
Co	120	110	110	90	70	70	60						
Cu	50	70	110	110	20	10	40						
f, at. %	19.0	18.0	18.0	20.0	55.0	20.0	41.0	15.4	16.4	14.5	18.6	18.8	29.6
No.	5							3					

Table 3. (Contd.)

Component	A(B)			SK		AT	SK	SpZ	PxK	A(B)	SpZ	PxK	A(B)
	137	138	139	U-14	U-15	U-16	U-17	U-18	U-20	150	156	157	158
SiO_2	50.07	49.60	53.22	45.30	42.94	44.91	42.07	42.14	45.44	51.25	45.33	49.45	52.18
TiO_2	1.04	0.72	0.80	0.18	0.43	0.57	0.50	0.48	0.80	1.11	0.55	0.83	1.14
Al_2O_3	14.30	12.54	14.93	2.91	6.57	6.99	6.48	6.62	10.00	14.50	7.09	10.89	14.18
Fe_2O_3	3.85	2.36	2.63	2.43	4.39	3.73	3.12	5.72	4.23	2.97	5.33	2.42	2.74
FeO	10.42	10.25	7.90	4.85	5.61	7.29	7.94	6.13	9.63	11.29	7.69	10.00	10.08
MnO	0.23	0.23	0.16	0.15	0.16	0.14	0.14	0.12	0.18	0.22	0.13	0.20	0.24
MgO	7.55	10.39	7.72	22.51	23.61	25.28	26.63	25.80	13.62	6.82	28.51	12.64	7.42
CaO	9.80	12.45	9.77	11.72	7.48	4.24	2.20	4.71	11.30	9.51	5.28	11.98	9.62
Na_2O	1.84	1.18	2.53	0.27	0.38	0.21	0.06	0.13	2.06	1.59	0.02	1.33	1.99
K_2O	0.77	0.20	0.24	0.02	0.03	0.05	0.01	0.01	0.14	0.61	0.01	0.17	0.28
H_2O^-	0.14	0.10	0.12	0.02	0.02	0.02	0.25	0.02	0.02	0.09	0.07	0.06	0.07
LOI	1.75	1.88	1.50	3.27	5.64	4.24	7.10	6.78	2.62	1.83	7.81	1.96	1.53
P_2O_5	0.14	0.07	0.10	0.03	0.03	0.03	0.03	0.04	0.06	0.13	0.07	0.09	0.12
CO_2				6.42	2.41	1.38	2.61	1.21	0.00				
S_{tot}				0.00	0.10	0.04	0.00	0.01	0.00				
Cr				1090	1980	2460	2870	2740	1090				
V				60	110	110	170	170	280				
Ni				660	1300	1600	1500	1400	550				
Co				80	140	140	140	140	120				
Cu				10	60	30	10	30					
f, at.%	50.8	40.1	42.7	14.8	18.6	19.2	17.2	19.7	35.5	53.4	19.7	35.1	48.7
No.	3			15						18	18		

Component	PilL	LB	AT		LMZ–CZ			PBK		SK	PilL	SK	
	U-59	U-36	U-37	U-58	9014a	9014a[2]	9014b[1]	U-60	WL-1	WL-3	WL-4	WL-5	WL-6
SiO_2	41.83	44.96	45.45	44.18	44.17	44.70	43.75	45.39	40.99	45.86	42.97	46.00	47.58
TiO_2	0.18	0.37	0.34	0.39	0.26	0.23	0.19	0.30	0.52	0.51	0.37	0.31	0.42
Al_2O_3	4.07	5.14	5.15	5.68	5.78	4.67	4.79	4.67	8.80	7.86	5.27	5.05	6.17
Fe_2O_3	5.30	6.54	6.26	5.05				4.22	4.10	4.28	4.44	2.44	2.67
FeO	3.54	5.17	4.48	4.68	14.16	14.57	13.54	5.64	5.80	6.99	5.86	6.31	6.45
MnO	0.11	0.15	0.14	0.13	0.30	0.36	0.26	0.14	0.13	0.17	0.15	0.15	0.16
MgO	31.28	23.30	24.19	25.87	27.48	29.49	31.60	25.11	23.78	21.38	27.84	27.72	22.78
CaO	2.45	7.58	6.96	6.32	7.70	5.83	5.78	7.56	6.65	7.42	4.90	4.71	7.74
Na_2O	0.04	0.10	0.08	0.09	0.13	0.13	0.07	0.24	0.66	0.56	0.20	0.19	0.92
K_2O	0.03	0.02	0.01	0.02	0.02	0.02	0.02	0.02	0.04	0.04	0.02	0.02	0.04
H_2O^-	0.63	0.36	0.53	0.40				0.42	0.36	0.13	0.24	0.12	0.13
LOI	10.25	5.72	6.13	6.63				5.68	6.95	4.08	7.03	6.41	4.40
P_2O_5	0.01	0.03	0.02	0.02				0.00	0.04	0.03	0.00	0.00	0.01
CO_2	0.19	0.16	0.19	0.22				0.14	0.08	0.19	0.19	0.58	0.11
S_{tot}	0.05	0.15	0.08	0.06				0.14	0.07	0.02	0.05	0.02	0.17
Cr	1780	2530	2120	2120	2191	2893	1530	2120	2670	2300	1890	2040	1980
V	110	170	110	170	135	160	109	110	250	210	0	170	145
Ni	2100	1400	1000	1200	1690	1570	1847	1300	990	1600	1900	1700	1200
Co	130	120	120	120	95	94	84	130	73	120	110	120	110
Cu		90	60	70	57	0.0	0.0	90	92	60	20	30	140
f, at.%	13.0	21.0	19.0	17.0	22.4	21.7	19.4	17.4	18.3	22.1	16.6	14.7	18.0
No.					11			11		Western Litsa			

Note: (ML) massive lava; (PilL) pillow lava; (LMZ) lower chilled margin; (CZ) cumulate zone; (SpZ) spinifex and (BZ) brecciated zones of differentiated flows; (LB) lava breccia; (AT) agglomerate tuff; (PK) peridotite komatiite; (PxK) pyroxenite komatiite; (SK) sheared komatiite; (PBK) porphyroblastic komatiite; and (A(B)) plagioamphibolite (metabasalt). *f*, at. % = $100(Fe^{2+} + Fe^{3+})/(Fe^{2+} + Fe^{3+} + Mg)$. No. is body number in the schematic map (Fig. 1). Analyses were performed by atomic absorption (samples U-5–U-60, chemical laboratory of the Geological Institute, Kola Research Center), XRF (Samples 130–158, 9014–9019; analytical laboratory of the Geological Institute, Karelian Research Center) and mass-spectrometry (Samples 9014–9019, ore elements; Granada University) methods.

Table 4. Chemical composition of komatiites from sills and host amphibolites (basalts) of the Ura Bay–Titovka structure (major elements in wt %, trace elements in ppm)

Component	PK	PK			PK			PK		A(B)	PK	
	U-7	U-8	U-9	U-10	U-24	U-56	U-57	U-21	U-22	U-23	9016	9019g
SiO_2	49.28	41.33	42.88	43.33	41.02	42.22	47.76	39.38	47.54	44.74	44.71	44.06
TiO_2	0.34	0.48	0.50	0.41	0.28	0.19	0.22	0.65	0.24	0.65	0.21	0.53
Al_2O_3	4.66	7.51	7.34	5.96	6.25	5.66	4.78	9.32	5.28	16.08	6.10	5.04
Fe_2O_3	2.58	5.51	5.72	6.37	4.78	4.70	2.01	4.80	4.25	3.79		
FeO	6.41	6.13	5.98	5.95	6.90	6.08	5.23	7.45	5.50	8.58	12.23	14.65
MnO	0.20	0.13	0.13	0.12	0.17	0.16	0.16	0.14	0.16	0.20	0.24	0.30
MgO	24.22	25.01	24.08	26.14	27.47	26.60	22.96	24.88	22.40	10.16	29.94	30.37
CaO	6.20	5.33	6.02	3.80	4.08	5.38	9.55	4.44	8.90	10.20	6.38	4.96
Na_2O	0.03	0.05	0.07	0.02	0.06	0.08	0.10	0.09	0.22	2.28	0.07	0.07
K_2O	0.04	0.01	0.01	0.01	0.02	0.02	0.02	0.01	0.02	0.31	0.02	0.02
H_2O^-	0.20	0.02	0.02	0.02	0.28	0.37	0.30	0.02	0.02	0.09		
LOI	5.63	7.06	6.95	6.85	7.27	6.90	4.68	8.41	5.31	2.03		
P_2O_5	0.02	0.03	0.03	0.02	0.05	0.02	0.01	0.06	0.03	0.08		
CO_2	0.00	0.98	0.00	0.00	0.45	0.90	1.14	0.00	0.00	0.14		
S_{tot}	0.00	0.15	0.06	0.36	0.06	0.16	0.37	0.00	0.01	0.00		
Cr	2050	2660	2460	460	2740	2390	1780	2260	1920	615	2949	1556
V	110	110	170	170	170	70	40	280	110	340	202	0.1
Ni	1200	1300	1400	1500	1200	1100	1700	1100	900	170	1621	2279
Co	80	100	130	100	140	150	120	120	80	100	102	104
Cu	0	50	100	160	60	65	100	0	20	10	4	5
f, at. %	16.8	19.9	20.6	20.0	18.5	17.8	14.7	20.9	18.9	39.8	18.8	21.3
No.	9				12			16			16	

peridotite and pyroxenite komatiites is plotted near the line with $CaO/Al_2O_3 = 1 : 1$ at total variations of this ratio from 0.5 to 1.7. For the subvolcanic bodies, variations in CaO/Al_2O_3 ratio can be explained by the mobility of Al_2O_3 and CaO during chloritization and serpentinization. For the volcanic rocks, these variations could be related to the combined effect of chloritization, amphibolization, and the latest carbonatization. The high CO_2 content, which serves as an indicator of carbonatization, may be accompanied by both an increase (to 1.65) or a decrease (to 0.37) in the CaO/Al_2O_3 ratio of the rocks. The porphyroblastic komatiites also exhibit considerable variations in CaO/Al_2O_3 ratio at the lowest CO_2 content.

In the diagram TiO_2–Al_2O_3 (Fig. 8a), most komatiites from the Ura Bay–Titovka structure are plotted between the lines $Al_2O_3/TiO_2 = 10$ and 20, and a few data points are plotted near the line $Al_2O_3/TiO_2 = 20$. The latter are grouped within the komatiite field of the Archean greenstone belts of western and central Karelia.

A different pattern is observed for komatiites from Kolmozero–Voron'ya. The komatiite lavas and spatially associated small intrusions are plotted on the line $Al_2O_3/TiO_2 = 10$, forming a field of Al-depleted rocks, whereas the stratigraphically higher komatiite dikes are clustered in the field of Al-undepleted rocks with $Al_2O_3/TiO_2 \geq 20$. Even a greater difference between the Ura Bay–Titovka and Kolmozero–Voron'ya komatiites is revealed in the diagram (FeO*)–MgO (Fig. 8b), where the former show a negative and latter exhibit a positive correlation between (FeO*) and MgO. This indicates different fractionation paths of the parental melts. For the rocks of the Kolmozero–Voron'ya structure, early olivine-controlled differentiation in deep-seated (transitional) chambers changed significantly the melt composition. For the Ura Bay–Titovka rocks, the compositional variations are mainly related to melt differentiation in lava flows or sills.

The volcanic and subvolcanic komatiites of the Ura Bay–Titovka structure show almost identical chondritic REE distributions at a regular increase of total REE with decreasing MgO (Tables 5, 6; Fig. 9), which is consistent with olivine fractionation. Some samples show a considerable decrease in La, Ce, and Eu contents and $(La/Sm)_N$ (0.6–0.9). Low $(La/Sm)_N$ is characteristic of Yilgarn-type Archean komatiites (0.4–0.8). However, it could be also related to REE redistribution

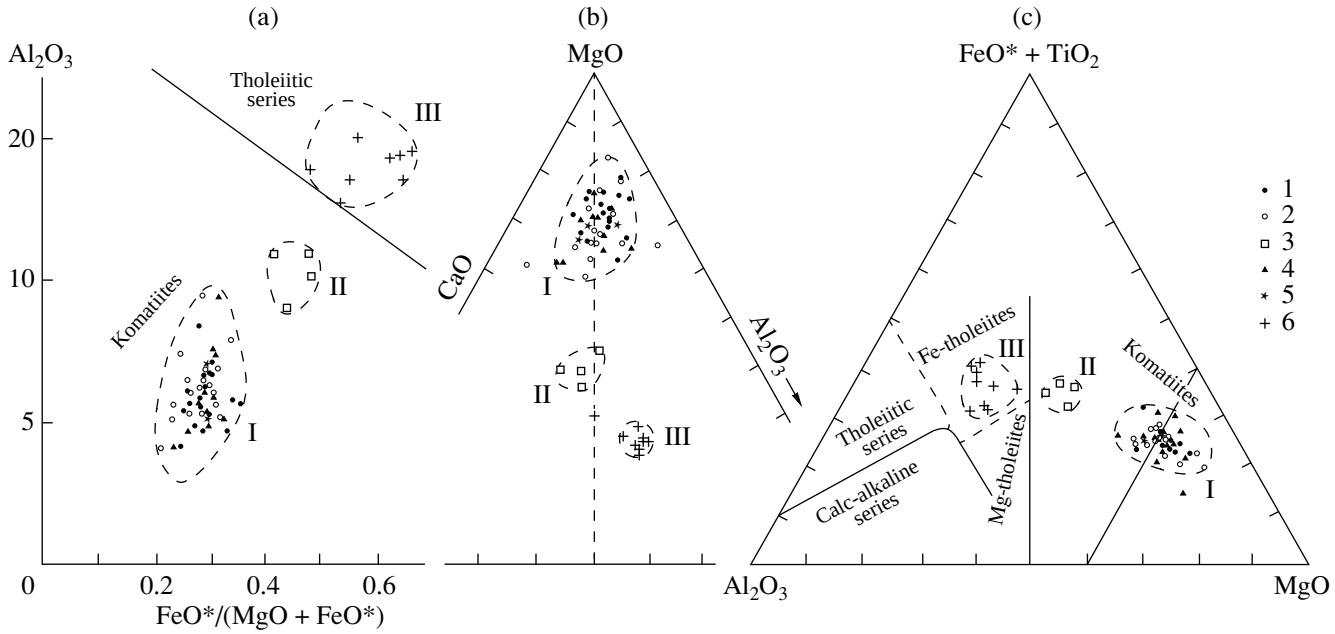

Fig. 7. Major components in the komatiites and spatially associated basalts of the Ura Bay–Titovka structure.
Peridotite komatiites from (1) differentiated lava flows and (2) pillow lavas; (3) pyroxenite komatiite; (4) subvolcanic rocks; (5) agglomerate tuffs; and (6) amphibolite. (c) Jensen (1976) diagram modified by Rickwood (1989). $FeO^* = FeO + 0.9Fe_2O_3$.

during metasomatism. A negative Eu anomaly is related mainly to plagioclase fractionation or metasomatic alteration accompanied by Eu removal. The absence of evidence of plagioclase crystallization and fractionation suggests that the partial LREE redistribution in the komatiites resulted from carbonatization.

Individual layered flows show no strong differentiation of major components (MgO, FeO*, and Al_2O_3) (Fig. 10). The high CO_2 content indicates that the increase of CaO content in the upper part of the cumulate zone is related to secondary carbonatization. Ni is differentiated increasing from the spinifex zone to cumulate rocks. Regular variations of most components were observed in the lower sheared chilled zone of a differentiated flow.

Judging from the section shown in Fig. 10, the composition of the spinifex zone does not correspond to the average composition of the lava flow and could not be used to characterize the parental melt. The massive rocks of the brecciated zone are more appropriate for this purpose. This agrees with inferences by other authors for komatiites from various regions (*Komatiites*, 1982).

Vrevsky *et al.* (1996) and Vrevsky and Krymsky (1997) studied the Sm–Nd isotope system in komatiites from the Karelian and Kola Archean greenstone belts.

Table 5. REE content in the rocks of komatiite association, Ura River (ppm)

Element	U-5	U-5a	U-15	U-18	U-20	U-8	U-9	U-10	U-21
La	0.50	0.70	1.20	0.50	1.50	0.60	1.1	0.40	1.00
Ce	2.00	3.00	4.00	2.00	5.00	2.00	4.00	2.00	3.00
Nd	2.00	3.00	3.00	2.00	4.00	2.00	3.00	2.00	3.00
Sm	0.51	0.80	0.82	0.75	1.50	0.65	1.00	0.60	1.10
Eu	0.13	0.28	0.32	0.21	0.05	0.17	0.26	0.11	0.21
Tb	0.10	0.20	0.20	0.20	0.40	0.20	0.20	0.20	0.20
Yb	0.60	0.79	0.70	0.75	1.23	0.58	0.92	0.62	0.97
Lu	0.09	0.12	0.11	0.11	0.17	0.06	0.14	0.09	0.14
MgO	27.7	25.3	23.6	25.8	13.6	25.0	24.1	26.1	24.9
La_N/Sm_N	0.6	0.5	0.9	0.4	0.6	0.6	0.7	0.4	0.6

Note: Measurements were carried out by INAA in the Geological Survey of Finland. See Tables 3 and 4 for number and location of samples.

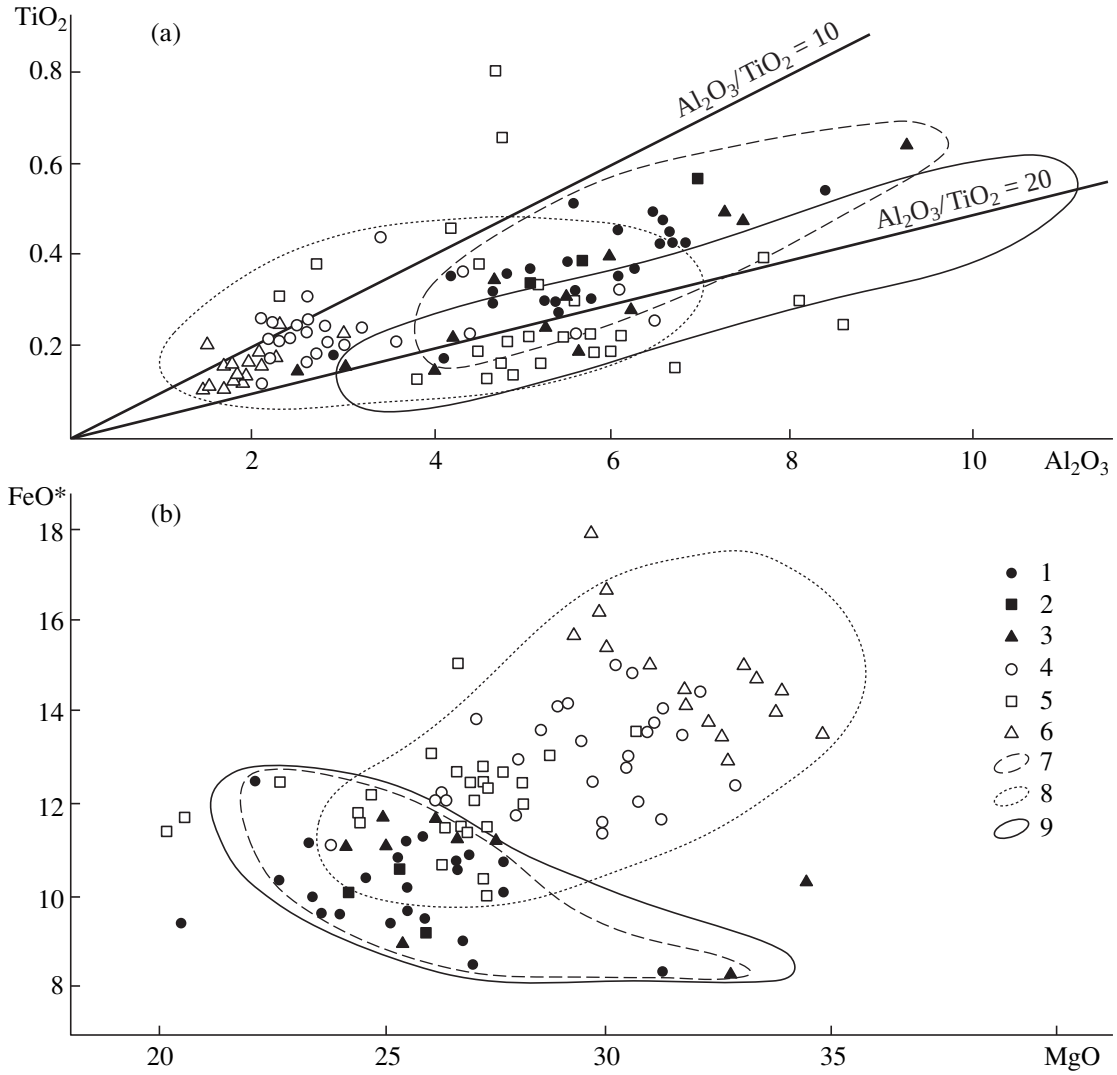

Fig. 8. TiO_2–Al_2O_3 (a) and FeO*–MgO (b) diagrams for the komatiites of the Northern Kola greenstone belt.
(1) Lava flows; (2) agglomerate tuffs and (3) sills of the Ura River; (4) lava flows; (5) dikes and (6) small intrusions of the Kolmozero–Voron'ya structure (Smolkin *et al.*, 1991a; Smolkin, 1992); compositional fields of the komatiites of the Ura Bay–Titovka (7) and Kolmozero–Voron'ya (8) structures; (9) compositional field of komatiites from the Sumozero–Kenozero, Vedlozero–Segozero, and Gimola–Kostomuksha greenstone belts of Karelia (*Komatiity…*, 1988).

Whole-rock samples from the Ura Bay (sample no. 9016), Polmos–Poros, Khizovaara, and Kostomuksha (n = 7) are plotted along a line corresponding to an age of 2779 ± 140 Ma, ε_{Nd} = +3.4 ± 0.5, and MSWD = 3.6. The komatiites show chondritic or slightly depleted REE distribution [$(Ce/Sm)_N$ = 0.92–1.09]. The age value obtained was believed to reflect the generation time of komatiite melts from a depleted source with ε_{Nd} = +3.4. This conclusion agrees with the general evolution of the Sm–Nd system in mantle rocks (Smolkin, 1997).

Recent U–Pb dating of the rocks from the Kolmozero–Voron'ya structure showed an age of 2828 ± 8 Ma for zircon from the quartz porphyries of the basalt–andesite–dacite sequence (Kudryashov *et al.*, 1998). This suggests that the age of underlying komatiites should be older than 2828 Ma and requires a refinement.

DISCUSSION

Genesis of the komatiite association. The data on the Northern Kola greenstone belt located within a granulite–greenstone terrane allow us to reconstruct the general sequence of ultramafic magmatism and physicogeographical environment of the formation of the komatiite association.

Owing to the Late Archean tectonic activization, the long-term erosion stage changed to the initiation of a greenstone belt and its subsequent opening in a protoriftogenic setting. The activity and depth of primary belt opening were different at various flanks. This is

Table 6. Contents of ore, trace, and rare-earth elements (ppm)

Element	9014a	9019g	Element	9014a	9019g
Cr	2192	1556	La	1.51	0.70
V	134.8	0.1	Ce	3.80	1.83
Ni	1690	2279	Pr	0.50	0.26
Co	95.3	104.1	Nd	2.39	1.04
Cu	56.6	5.0	Sm	0.80	0.32
Zn	63.5	43.8	Eu	0.27	0.08
Rb	4.3	0.0	Gd	0.89	0.27
Sr	74.7	12.9	Tb	0.16	0.05
Ba	1.6	0.0	Dy	1.26	0.39
Nb	1.1	0.7	Ho	0.25	0.08
Ta	0.1	0.1	Er	0.74	0.23
Zr	4.0	3.0	Tm	0.11	0.03
Y	7.4	2.33	Yb	0.67	0.18
Hf	0.2	0.1	Lu	0.10	0.03
			La_N/Sm_N	1.15	1.35
			Cd_N/Yb_N	1.07	1.20

Note: See Tables 3 and 4 for number and location of samples. Analyses were carried out by ICP-MS in the Granada University, Spain, analyst F. Bea.

confirmed by the varying thickness of the komatiite–basalt sequences and relations between komatiites and basalts. The longest period of komatiite magmatism within the eastern part of the belt (western part of the Kolmozero–Voron'ya structure) was presumably related to the activity of deep-seated Al-depleted mantle sources and transitional chambers, which provided a relatively wide spectrum of ultramafic rocks. The deep-seated differentiation was controlled mainly by olivine crystallization. Within the western part of the belt (Ura Bay–Titovka structure), the komatiite–basalt magmatism was less prolonged and originated from a shallower Al-undepleted source; thus producing nearly undifferentiated or slightly differentiated melts.

The presence of komatiite pillow and ball lavas and vague graded bedding in the agglomerate tuffs (together with the presence of pillow basalts in the sequences) indicate subaqueous eruptions of komatiite magmas. The spatially associated differentiated flows with spinifex zones were formed under the same conditions. The lavas with clastic structures are breccias formed by the breaking of a cooled rind of the lava flow during its relatively rapid movement. The lack of amygdaloidal rocks suggests that the komatiite magmas were fluid-undersaturated. The deposition of the scarce agglomerate tuffs was related to local phreatic explosions, which accompanied occasionally subaqueous eruptions.

The sequences described were formed at various distances from volcanic centers. The sequences composed of individual thin poorly differentiated flows were formed relatively far from volcanic centers. The complex thick sequences with repeated alternation of volcanic facies were formed near the vents. In general, the rocks are products of areal volcanism with numerous subaqueous volcanic edifices, no more than a few hundred meters in height.

Mantle genesis. On the basis of the data obtained, we calculated the composition of parental (primary) magma and estimated the conditions of its generation. Our calculations are approximate because of metamorphic alterations.

The primary MgO content of the erupted magmas was calculated on the basis of average compositions of relict chilled zones and flowtop breccias. The results were checked by calculations of olivine–melt equilibrium. The Ura Bay komatiites contain no relicts of the earliest high-Mg olivine. Based on the suggestion that the compositions of the early olivine from the Ura Bay and Kolmozero–Voron'ya structures were similar, the most magnesian olivine (*Fo* 91.5–93) from the Kolmozero–Voron'ya lava flows (Smolkin *et al.*, 1991a) was used for calculations. Taking the distribution coefficient of Mg and Fe^{2+} between olivine and melt,

$$K_D^{Ol-Liq} = (Mg/Fe^{2+})_{Liq}/(Mg/Fe^{2+})_{Ol} = 0.31 \quad (1)$$

(Beattie *et al.*, 1991), we obtain that such an olivine could be in equilibrium with a primary melt containing 25–26 wt % MgO. This value agrees well with the average (nine samples) MgO content of rocks from the chilled and brecciated zones (MgO = 26.05 ± 2.47 wt %).

Al-undepleted komatiites (Yilgarn or Munro-type) result from high-degree mantle melting with olivine as a main liquidus phase and an olivine–orthopyroxene restite at pressures <5 GPa (Arndt, 1976; Girnis *et al.*, 1987). This allows us to use the partition coefficients of elements between olivine (*Ol*), orthopyroxene (*Opx*), and melt (*Liq*) for the modeling of equilibrium melting.

The modeling of partial melting of a mantle source was carried out using the formula of Shaw (1970)

$$C_L = C_0/[D + F(1 - D)], \quad (2)$$

where C_0 is the concentration in the original material, C_L is the concentration of the element in the liquid, F is the weight fraction of melt produced by partial melting, D is the bulk partition coefficient for the solid residuum calculated by the formula

$$D = W_1K_{D1} + W_2K_{D2} + \ldots W_iK_{Di}, \quad (3)$$

where W_i is the content of mineral i (1…i) and K_{D1} is the partition coefficient of the element for mineral i (1…i).

For calculations, we used K_D values for komatiites, ultramafic, and mafic rocks (Table 7). Modeling showed that melts most similar to natural komatiites can be derived by 50–60% equilibrium melting of mantle pyrolite. This conclusion is in good agreement with the experimental investigations of Archean komatiites from Karelia (Girnis *et al.*, 1987) and modeling of the

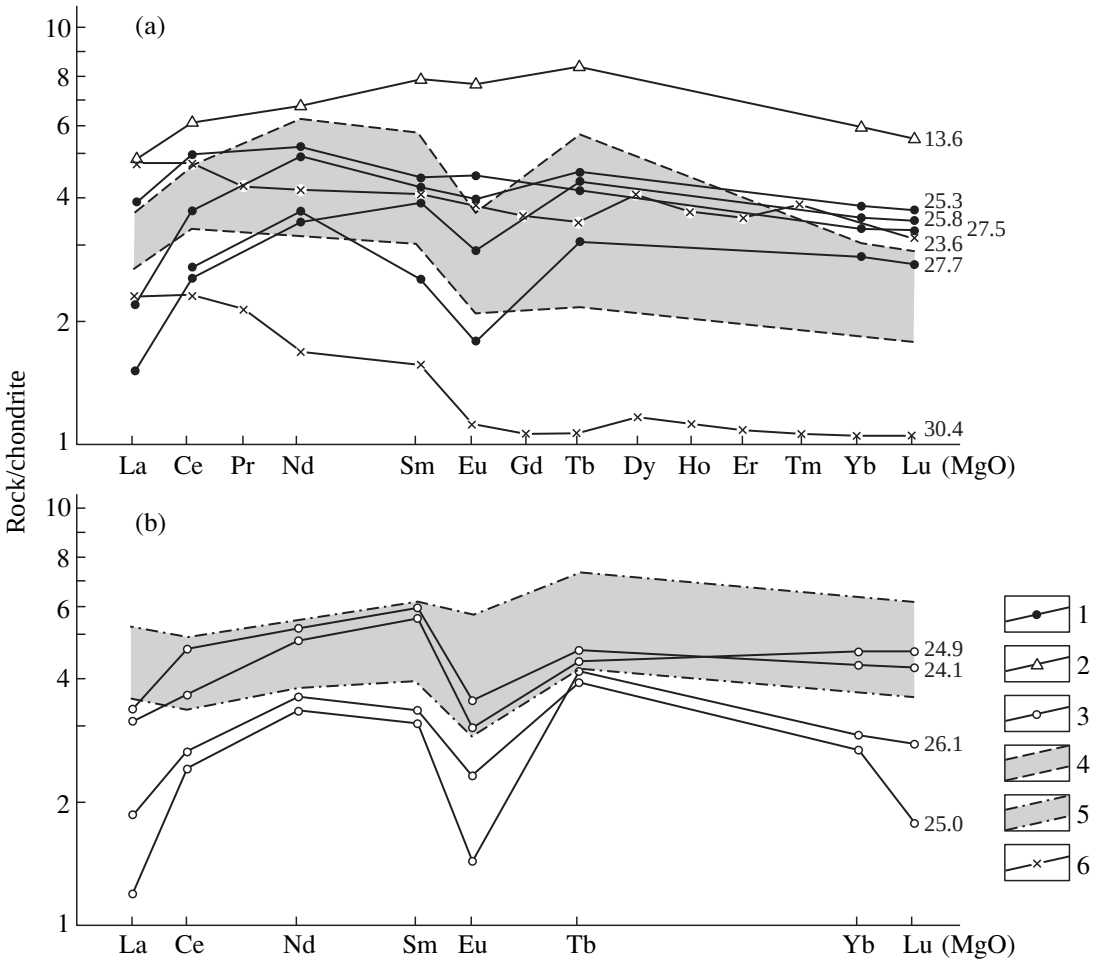

Fig. 9. Chondrite-normalized REE patterns for the volcanic (a) and subvolcanic (b) komatiites. REE contents were measured by INAA and mass spectrometry.

(1) Peridotite and (2) pyroxenite komatiite; (3) komatiite from sills; (4–5) peridotite komatiite from lava flows (4), dikes and small intrusions (5) of the Kolmozero–Voron'ya structure (Smolkin, 1992); (6) mass spectrometry data.

generation conditions of komatiites from Norway (Barnes and Often, 1990) and western Karelia (Puchtel *et al.*, 1998).

The liquidus temperatures of erupted komatiites were estimated by the experimentally derived equation for the dependence of temperature on MgO content (Nisbet *et al.*, 1993):

$$T_{Liq},°C = 1400\ [(MgO - 20) \times 20]. \quad (4)$$

We calculated the temperature of erupted melt (T_{Liq},°C) and potential temperature (T_{pot},°C), which is the temperature of the source in the case of its adiabatic ascent to the surface without melting. The potential temperature differ from that in the initial mantle chamber and was calculated using the equation of McKenzie and Bickle (1988):

$$T_{pot},°C = 1382.5 + 2.8046T_{Liq} - 0.00049671(T_{Liq})^2. \quad (5)$$

Using the average temperature values (1521 ± 50, 1549.6, and 1589.8°C) for the samples studied, the temperature in the source was calculated as 1734 ± 62°C:

Sample	MgO, wt %	T_{Liq}, °C	T_{pot}, °C
Average	26.05 ± 2.47	1521 ± 50	1734 ± 62
9014a-1	27.48	1549.6	1770.7
9014a-2	29.49	1589.8	1820.8

Thus, we estimated the temperature of erupted komatiites with an average MgO content of 26.05 ± 2.47 wt % as 1521 ± 50°C. This is nearly 200°C lower than the potential temperature of the deep source. The increase of MgO content to 29.49 wt % (sample 9014a-2) results in a temperature increase for erupted melts to 1590°C. According to experimental data (Arndt, 1976; Girnis *et al.*, 1987; Smolkin, 1992), olivine is the only low-pressure liquidus phase at such a temperature range. Therefore, melt differentiation is controlled mainly by the composition and abundance of olivine.

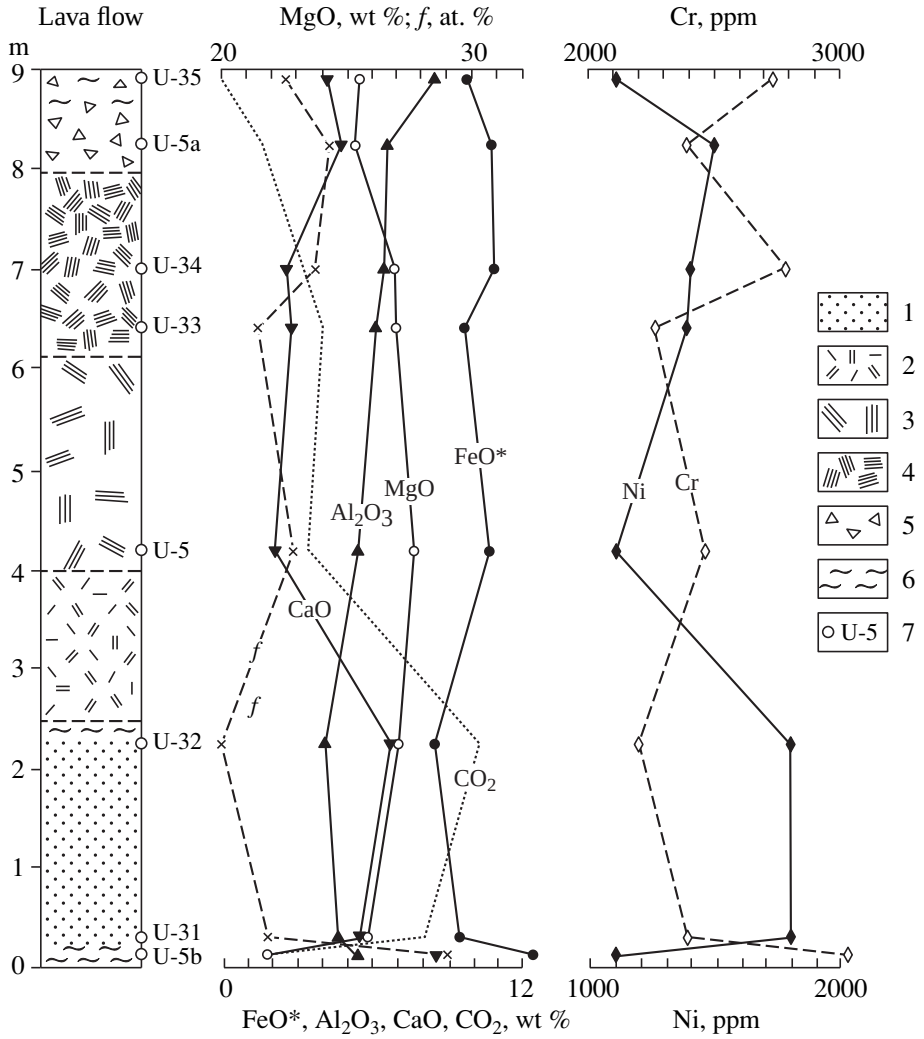

Fig. 10. Distribution of rock-forming and ore components in the differentiated komatiite flow (Fig. 1, no. 6).
(1) Cumulate zone; (2) scattered olivine spinifex; (3) coarse plated olivine spinifex; (4) plated–pocket olivine spinifex; (5) brecciated zone; (6) sheared zone; and (7) sample number. FeO* = FeO + 0.9Fe_2O_3; $f = (Fe^{2+} + Fe^{3+})/(Mg + Fe^{2+} + Fe^{3+})$, at. %.

Experimental investigations of komatiite crystallization at atmospheric pressure demonstrated that the temperature decrease to 1400°C resulted in spinifex textures formed by high-Mg olivine (*Fo* 92–94%) (Smolkin, 1992). A subsequent temperature decrease prevented spinifex growth and higher Fe euhedral olivine crystallized. Spinel began to crystallize at 1250°C. Such a crystallization sequence of komatiite melt indicates that the lower cumulate zone was formed later than the spinifex zone, in contrast to the model proposed by Arndt (1977, 1986).

The CaO/Al_2O_3 ratio depends strongly on pressure in the komatiite source. If the liquidus assemblage is represented by *Ol* + *Opx* + *Cpx* + *Gr*, the CaO and Al_2O_3 contents in the melt versus pressure can be expressed as the third order polynomial (Herzberg, 1995):

$$\mathrm{CaO\ (wt\ \%)} = 16.0811 - 2.0724P + 0.1322P^2 - 0.0018P^3, \quad (6)$$

$$\mathrm{Al_2O_3\ (wt\ \%)} = 22.8581 - 4.0110P + 0.2703P^2 - 0.0061P^3, \quad (7)$$

where *P* is pressure in GPa.

The best agreement between the calculated and experimental data was established at 2.5–6 GPa. Since the komatiites experienced high-grade metamorphism and secondary carbonation, the pressure calculated on the basis of CaO content can be overestimated. Therefore, more reliable data can be obtained using Al_2O_3 content. Below we present the calculated pressure in the mantle source with a garnet residue.

Sample	Al_2O_3, wt %	*P*, GPa	CaO, wt %	*P*, GPa
Average	5.92 ± 1.1	7.01 ± 0.8	5.66 ± 2	9.7 ± 3
9014a-1	5.78	7.13	7.70	6.50
9014a-2	4.67	8.34	5.83	9.79

Table 7. Results of the calculation of partial melting of mantle pyrolite

Component	Sample 9014a	Model 1	Model 2	Pyrolite[1]	K_D^{Ol} [2]	K_D^{Opx} [2]
TiO_2	0.26	0.30	0.30	0.201	0.024	0.11
MgO	27.48	–	–	37.8	–	–
Cr	2191.39	2169	2439	2625	0.5	2.8
Ni	1689.56	1507	1531	1960	2	1
Co	95.23	107	107	105	0.92	1
Nb	1.14	1.1	1.0	0.658	0.0001	0.027
Zr	3.95*	20.7	17.5	10.50	0.008	0.021
Y	7.42	7.9	7.1	4.30	0.021	0.19
La	1.51	1.294	1.079	0.648	0.0001	0.0019
Ce	3.80	3.345	2.788	1.675	0.0001	0.0035
Pr	0.50	0.507	0.422	0.254	0.0001	0.0035
Nd	2.39	2.487	2.076	1.250	0.0001	0.013
Sm	0.80	0.791	0.665	0.406	0.0006	0.063
Eu	0.27	0.300	0.252	0.154	0.0007	0.059
Gd	0.89	1.058	0.889	0.544	0.001	0.069
Tb	0.16	0.186	0.158	0.099	0.002	0.16
Dy	1.26	1.269	1.078	0.674	0.003	0.15
Ho	0.25	0.265	0.229	0.149	0.005	0.3
Er	0.74	0.795	0.684	0.438	0.008	0.24
Yb	0.67	0.755	0.661	0.441	0.019	0.39
Lu	0.10	0.104	0.093	0.067	0.03	0.67

Note: Models 1 and 2 show 50 and 60% melting of primitive mantle or pyrolite, respectively; equilibrium residue is $0.6Ol + 0.4Opx$.

* Zr content in the rocks ranges between 3 and 28 ppm.

[1] after McDonough and Sun (1995); [2] Cr, Ni, Co, and TiO_2 are after Barnes (1985), Y, Zr, Nb, and REE contents, from Snyder *et al.* (1996).

Using the calculated values of potential temperature in the source, we estimated the thickness of the Earth's crust from the formula of McKenzie and Bickle (1988):

$$T_{pot},°C = 1177.3 + 38.080(\ln T_{crust}) + 3.4131(\ln T_{crust})^2 + 6.0121(\ln T_{crust})^3, \quad (8)$$

where T_{pot},°C is the potential temperature and T_{crust} is the thickness of the crust (km).

Sample	T_{crust}, km
Average T_{pot}, °C (1734 ± 62)	49.98 ± 9
9014a-1	55.56
9014a-2	63.74

These estimates agree with the results of Puchtel *et al.* (1998) for the Vedlozero–Segozero (58–65 km) and Gimola–Kostomuksha (54 km) greenstone belts. It should be noted that the estimates of crust thickness are approximate, because the real tectonic setting, including spreading rate, were not taken into consideration in the calculations.

For comparison, similar calculations of temperature, pressure, and crust thickness were carried out for the komatiites of Karelia (Kamennoe ozero, Koikary, Palaselga, Sovdozero, Khautovaara, Kostomuksha, and Khizovaara) and Finland (Kuhmo and Tipasjarvi). The temperatures of erupted lavas ranged between 1440 and 1600°C; the potential temperatures in the source, 1700–1850°C; pressure calculated from Al_2O_3 content, from 4.9 to 7.2 GPa, and the crust thickness, 35–65 km. With respect to these parameters, the Ura Bay komatiites are most similar to the komatiites of Central Karelia (Koikary and Palaselga) and Finland (Tipasjarvi).

The data obtained suggest that the primary melts were generated at depths of 220–260 km at a potential temperature of about 1735°C. The thickness of the crust was 50–64 km. The magma erupted in subaqueous conditions at a temperature of about 1550°C with olivine as only a liquidus phase without preliminary differentiation in transitional chambers.

Metamorphism. The reconstruction of conditions of porphyroblast development in the komatiites of the Ura Bay–Titovka structure gives a clue for understanding metamorphic processes. The fayalite content of olivine

in the magmatic system is a function of parental melt composition. This defines a distinct positive correlation between Fe proportions in olivine and the host rock. However, the olivine porphyroblasts studied do not show such a correlation and are enriched in FeO and MnO with respect to groundmass (Tables 1, 3; Fig. 6). This and the above-mentioned mineralogical data suggest a secondary metamorphic origin of the porphyroblasts.

According to the data of Belyaev and Petrov (1991), regional metamorphism within the northern Kola region occurred in three stages: Late Lopian, Sumian, and Svecofennian. The first stage within the Northern Kola greenstone belt corresponded to low-grade amphibolite facies, the second stage within the belt and its framing corresponded to high-grade amphibolite facies, and the third stage produced metamorphic zonation from amphibolite to prehnite–pumpellyite facies. According to our data, the first stage resulted in the development of the chlorite (clinochlore)–tremolite (± serpentine–carbonate–magnetite) assemblage after komatiites. The relicts of primary olivine preserved because of the irregular character of metamorphic alterations.

Based on the calculation of normative mineral composition, the metamorphic reaction of the first stage can be written as

$$\underset{\text{forsterite}}{4Mg_2SiO_4} + \underset{\text{enstatite}}{10MgSiO_3} + \underset{\text{anorthite}}{2CaAl_2Si_2O_8}$$
$$+ \underset{\text{diopdide}}{2CaMgSi_2O_6} + 10H_2O = \underset{\text{tremolite}}{2Ca_2Mg_5Si_8O_{22}(OH)_2} \quad (9)$$
$$+ Mg_6Si_4O_{10}(OH)_8 \times \underset{\text{clinoclore}}{(Mg_4Al_2)(Si_2Al_2)O_{10}(OH)_8}.$$

The formation of olivine porphyroblasts occurred simultaneously and (or) somewhat later than tectonic movement and was related to the second metamorphic stage. The formation of metamorphic olivine is usually explained by deserpentinization (Vance and Dungan, 1977; Velinskii and Bannikov, 1986) or olivine development after chlorite (Oliver *et al.*, 1972, Stamateloupoulou-Seymour and Francins, 1980; Peltonen, 1990). Deserpentinization is widespread in Alpine-type ultramafic rocks. It is caused mainly by a temperature increase and produces high-Mg olivine (Vance and Dungan, 1977; Velinskii and Bannikov, 1986).

However, in our case, the development of secondary olivine during deserpentinization is highly improbable, because the porphyroblast-bearing komatiites do not contain serpentine, while olivine shows high FeO content. The reaction of olivine formation by chlorite replacement (Jenkins and Chernovsky, 1986) also cannot be used because of the absence of orthopyroxene, spinel, or cordierite in the rocks studied.

Judging from the compositions of mineral inclusions in the olivine porphyroblasts and compositions of minerals in the host groundmass (Table 1, 2), the formation of neomorphous olivine can be described by the following reaction:

$$\underset{\text{antigorite}}{3(Mg_{0.85}Fe_{0.15})_6Si_4O_{10}(OH)_8}$$
$$\times \underset{\text{amesite}}{3(Mg_{0.85}Fe_{0.15})_4Al_2(Si_2Al_2)O_{10}(OH)_8} \text{ [clinochlore]}$$
$$= \underset{\text{olivine}}{3(Mg_{0.75}Fe_{0.25})_2SiO_4} + \underset{\text{antigorite}}{2(Mg_{0.875}Fe_{0.125})_6Si_4O_{10}(OH)_8} \quad (10)$$
$$\times \underset{\text{amesite}}{3(Mg_{0.875}Fe_{0.125})_4Al_2(Si_2Al_2)O_{10}(OH)_8} \text{ [clinochlore]}$$
$$+ SiO_2\uparrow + 4H_2O\uparrow.$$

In reaction (10), the clinochlore composition is expressed in serpentine (antigorite) and chlorite (amesite) end-members. This reaction proceeds in a relatively narrow temperature range (T = 650–700°C). It causes the decrease of FeO content in clinochlore, because part of Fe is consumed by newly-formed olivine during prograde metamorphism. At temperatures above 700°C, Mg-chlorites are unstable and decompose into forsterite, orthopyroxene, and spinel (Jenkins and Chernosky, 1986). This process can be exemplified by the metamorphic assemblage that formed during chlorite replacement by olivine in the metavolcanic rocks of Finland (Peltonen, 1990). The reaction of olivine regeneration (10) is consistent with the amphibolite-facies metamorphic conditions of the Western Litsa–Titovka mafic rocks:

T = 570–630°C and P = 450–650 MPa (Belyaev *et al.*, 1977).

The third, retrograde metamorphic stage was responsible for the formation of iddingsite or bowlingite rims around olivine porphyroblasts.

CONCLUSION

(1) The Kola region is one of the rare examples of granulite–greenstone terranes. Unlike more widespread greenstone belts, they contain granulite complexes and are characterized by higher-grade metamorphism of volcanogenic and sedimentary rocks of greenstone belts, which hampers the reconstruction of their genesis. A NW-trending Late Archean greenstone belt, about 300 km long, was recognized within the Kola region. Its western part (middle reaches of the Ura, Titovka, and Western Litsa rivers) contains metamorphosed ultramafic rocks, which initially composed lava flows, agglomerate tuff horizons, lava breccias of variable thickness and structure, and sill-like bodies. In terms of texture, structure, petrochemistry, and mineralogy, these rocks are classified as volcanic and subvolcanic komatiites. The volcanic komatiites were originated owing to eruptions or phreatic explosions from

numerous volcanic edifices in subaqueous environments. A decrease in fluid pressure led to predominant development of subvolcanic rocks.

(2) Geochemically, the rocks studied are most similar to Al-undepleted komatiites, but have a somewhat lower Al_2O_3/TiO_2 ratio. The potential temperature and pressure in the mantle source is estimated to be 1730°C and 7–8 GPa, respectively. The crust was about 50–64 km thick. The temperature of erupted komatiites was about 1520°C.

(3) Komatiites experienced intense three-stage metamorphism under amphibolite (low and high-grade) and greenschist facies. The development of porphyroblasts in the komatiites occurred simultaneously with dynamometamorphism. Secondary olivine resulted from chlorite decomposition at a local temperature increase to 650–700°C.

ACKNOWLEDGMENTS

We are grateful to A.B. Vrevsky (Institute of Precambrian Geology and Geochemistry, St. Petersburg) and A.V. Girnis (Institute of Geology of Ore Deposits, Petrography, Mineralogy, and Geochemistry, Moscow) for critical comments and F. Bea (Granada University, Spain) for carrying out analytical investigations.

This study was supported by the Russian Foundation for Basic Research (project no. 98-05-64276).

REFERENCES

Arndt, N.T., Differentiation of Komatiite Flows, *J. Petrol.*, 1986, vol. 27, pp. 279–301.

Arndt, N.T., Melting Relation of Ultramafic Lavas (Komatiites) at 1 Atm and High Pressure, *Carnegie Inst. Washington, Year Book 1975/1976*, 1976, pp. 555–562.

Arndt, N.T., Naldrett, A.J., and Pyke, D.R., Komatiitic and Iron-rich Tholeiitic Lavas of Munro Township, Northeast Ontario, *J. Petrol.*, 1977, vol. 18, pp. 319–369.

Arndt, N.T., Thick, Layered Peridotite–Gabbro Lava Flows in Munro Township, Northeast Ontario, *Can. J. Earth Sci.*, 1977, vol. 14, pp. 2620–2637.

Arutyunyan, L.A., Sargsyan, G.O., and Smolkin, V.F., On the Nickel Potential of Olivine Crystallizing in Silicate and Sulfide–Silicate Systems, in *Nikelenosnost' bazit–giperbazitovykh kompleksov Ukrainy, Urala, Sibiri i Dal'nego Vostoka* (Nickel Potential of Mafic–Ultramafic Complexes of Ukraine, Urals, Siberia, and the Soviet Far East), Apatity: Akad. Nauk SSSR, Kol'skii Nauch. Tsentr, 1988, pp. 78–81.

Arzamastsev, A.A., Kaverina, V.A., and Polezhaeva, L.I., *Daikovye porody Khibinskogo massiva i ego obramleniya* (Dike Rocks of the Khibina Massif and Its Framing), Apatity: Akad. Nauk SSSR, Kol'skii Nauch. Tsentr, 1988.

Barnes, S.J., The Petrography and Geochemistry of Komatiite Flows from the Abitibi Greenstone Belt and a Model for Their Formation, *Lithos*, 1985, vol. 18, pp. 241–270.

Barnes, S.J., Gorton, M.P., and Naldrett, A.J., A Comparative Study of Olivine and Clinopyroxene Spinifex Flows from Alexo, Abitibi Greenstone Belt, Ontario, Canada, *Contrib. Mineral. Petrol.*, 1983, vol. 83, pp. 293–308.

Barnes, S.J. and Often, M., Ti-rich Komatiites from Northern Norway, *Contrib. Mineral. Petrol.*, 1990, vol. 105, pp. 42–54.

Beattie, P., Ford, C., and Russel, D., Partition Coefficients for Olivine–Melt and Orthopyroxene–Melt Systems, *Contrib. Mineral. Petrol.*, 1991, vol. 109, pp. 221–224.

Belyaev, O.A., Bushmin, S.A., Volodichev, V.A., *et al.*, *Fatsii metamorfizma vostochnoi chasti Baltiiskogo shchita* (Metamorphic Facies in the Eastern Part of the Baltic Shield), Leningrad: Nauka, 1977.

Belyaev, O.A. and Petrov, V.P., Main Stages in the Tectono-Metamorphic Development of the Earth's Crust in the Kola Metamorphic Belt, Baltic Shield), *Dokembrii Severnoi Evrazii. Mezhdunarodnoe soveshch.* (Int. Conf. Precambrian of North Eurasia), St. Petersburg: Inst. Geol. Geokhronol. Dokembriya, Ross. Akad. Nauk, 1997, p. 12.

Borisova, V.V., Borisov, A.E., and Smolkin, V.F., New Manifestation of Komatiite Volcanism in the Kola Peninsula, *Dokl. Akad. Nauk SSSR*, 1991, vol. 316, no. 1, pp. 196–199.

Borisova, V.V., Borisov, A.E., Smolkin, V.F., and Rezhenova, S.A., The Genesis of Porphyroblastic Olivine in Komatiites of the Kola Peninsula, *Zap. Vseross. Mineral. O-va*, 1998, no. 2, pp. 63–71.

Girnis, A.V., Ryabchikov, I.D., and Bogatikov, O.A., *Genezis komatiitov i komatiitovykh bazal'tov* (Genesis of Komatiites and Komatiitic Basalts), Moscow: Nauka, 1987.

Gordienko, V.V. and Charikov, A.V., The Ura River Granite Pegmatite Field, Kola Peninsula: Regional Mineralogical and Geochemical Zonation and Its Quantitative Description, in *Voprosy geokhimii i tipomorfizm mineralov* (Geochemical Problems and Mineral Typomorphism), 1998, no. 5, St. Petersburg: St. Petersburg Gos. Univ., pp. 151–163.

Hanski, E., Komatiitic and Tholeiitic Metavolcanics of the Sivikkovaara Area in the Archean Kuhmo Greenstone Belt, Eastern Finland, *Bull. Geol. Soc. Finland*, 1980, vol. 52, pp. 67–100.

Herzberg, C., Generation of Plume Magma through Time: an Experimental Perspective, *Chem. Geol.*, 1995, vol. 126, pp. 1–16.

Jahn, B.M., Auvray, B., Blais, S., *et al.*, Trace Element Geochemistry and Petrogenesis of Finnish Greenstone Belts, *J. Petrol.*, 1980, vol. 21, pp. 201–244.

Jenkins, D.M. and Chernosky, J.V., Jr., Phase Equilibria and Crystallochemical Properties of Mg-Chlorite, *Am. Mineral.*, 1986, vol. 71, nos. 7–8, pp. 924–936.

Jensen, L.S., A New Cation Plot for Classifying Subalkalic Volcanic Rocks, *Ontario Div. Mines. Misc.*, 1976, vol. 66, pp. 1–22.

Kol'skaya sverkhglubokaya. Nauchnye rezul'taty i opyt issledovanii (The Cola Superdeep Hole: Scientific Results and Investigation Experience), Orlov, V.P. and Laverov, N.P., Eds., Moscow: TEKhNONEFT'GAZ, 1998.

Komatiites, Arndt, N.T. and Nisbet, F.G., Eds., London: Allen and Unwin, 1982.

Komatiity i vysokomagnezial'nye bazal'ty rannego dokembriya Baltiiskogo shchita (Komatiites and Highly Magnesian Basalts of the Early Precambrian in the Baltic Shield), Bogatikov, O.A., Ed., Leningrad: Nauka, 1988.

Kudryashov, N.M., Zozulya, D.R., and Apanasevich, E.A., Age and Formation Conditions of Quartz Porphyries in the Kolmozero–Voron'ya Greenstone Belt (Kola Peninsula), *Problemy genezisa magmaticheskikh i metamorficheskikh porod. Tez. Mezhdunarodnoi konf.* (Int. Conf. on Problems of

Igneous and Metamorphic Rock Genesis), St. Petersburg: St. Petersburg Gos. Univ., 1998, pp. 105–106.

Levchenkov, O.A., Levsky, L.K., Nordgulen, O., *et al.*, U–Pb Zircon Ages from Sorvaranger, Norway, and the Western Part of the Kola Peninsula, Russia, *Geology of the Eastern Finnmark–Western Kola Peninsula Region. Norg. Geol. Unders. Spec. Publ.*, Roberts, D. and Nordgulen, O., Eds., 1995, no. 7, pp. 29–48.

McDonough, W.F. and Sun, S.S., The Composition of the Earth, *Chem. Geol.*, 1995, vol. 120, pp. 223–253.

McKenzie, D.P. and Bickle, M.J., The Volume and Composition of Melt Generated by Extension of the Lithosphere, *J. Petrol.*, 1988, vol. 29, pp. 625–679.

Metallogenicheskaya evolyutsiya arkheiskikh zelenokamennykh poyasov Karelii (Metallogenic Evolution of Archean Greenstone Belts in Karelia), Lazarev, Yu.I., Ed., St. Petersburg: Nauka, 1993, part 1.

Mitrofanov, F.P., *Geologicheskaya karta Karelo-Kol'skogo regiona. Masshtab 1 : 500000* (Geological Map of the Karelia–Kola Region, Scale 1 : 500000), Apatity, 1996.

Nesbitt, R.W., Jahn, B.M., and Purvis, A.S., Komatiites: an Early Precambrian Phenomenon, *J. Volcanol. Geotherm. Res.*, 1982, vol. 14, pp. 31–45.

Nisbet, E.G., Cheadle, M.J., Arndt, N.T., and Bickle, M.J., Constraining the Potential Temperature of the Archean Mantle: a Review of Evidence from Komatiites, *Lithos*, 1993, vol. 30, pp. 291–307.

Often, M., The Early Proterozoic Karasjok Greenstone Belt, Norway: A Preliminary Description of Lithology, Stratigraphy and Mineralization, *Geology of Finmark. Bull. Norg. Geol. Unders.*, Trondheim, 1985, no. 403, pp. 75–88.

Oliver, R.L., Nesbitt, R.W., Hansen, D.M., and Franzen, N., Metamorphic Olivine in Ultramafic Rocks from Western Australia, *Contrib. Mineral. Petrol.*, 1972, vol. 36, no. 4, pp. 335–342.

Peltonen, P., Metamorphic Olivine in Picritic Metavolcanics from Southern Finland, *Bull. Geol. Soc. Finl.*, 1990, vol. 62, pp. 99–114.

Plaksenko, A.N. and Smolkin, V.F., Typomorphism of Accessory Chromian Spinels in Highly Magnesian Volcanics, *Int. Geol. Rev.*, 1990, vol. 32, pp. 244–259.

Pozhilenko, V.I., Smolkin, V.F., and Sharov, N.V., Seismo–Geological Models of the Earth's Crust in the Laplandia–Pechenga Area, in *Seismogeologicheskaya model' litosfery Severnoi Evropy: Laplandsko-Pechengskii raion* (Seismo–Geological Model of the Lithosphere in Northern Europe: The Lapland–Pechenga Area), Sharov, N.V., Ed., Apatity: Ross. Akad. Nauk, Kol'skii Nauch. Tsentr, 1997, pp. 181–208.

Pozhilenko, V.I., Zhamaletdinov, A.A., Smolkin, V.F., and Sharov, N.V., *Seismogeologicheskaya model' zemnoi kory po severnomu uchastku profilya 1-EV* (Seismo–Geological Models of the Earth's Crust in the Northern Section of Profile 1-EV), Sharov, N.V., Ed., Apatity: Ross. Akad. Nauk, Kol'skii Nauch. Tsentr, 1998, pp. 10–50.

Puchtel, I.S., Hofmann, A.W., Mezger, K., *et al.*, Oceanic Plateau Model for Continental Crustal Growth in the Archean: A Case Study from the Kostomuksha Greenstone Belt, NW Baltic Shield, *Earth Planet. Sci. Lett.*, 1998, vol. 155, pp. 57–74.

Radchenko, A.T., Balaganskii, V.V., Basalaev, A.A., *et al.*, *Ob"yasnitel'naya zapiska k geologicheskoi karte severo-vostochnoi chasti Baltiiskogo shchita masshtaba 1 : 500000* (Explanatory Notes to the Geological Map of the Northeastern Part of the Baltic Shield, Scale 1 : 500000), Apatity: Ross. Akad. Nauk, Kol'skii Nauch. Tsentr, 1994.

Rickwood, P.C., Boundary Lines within Petrologic Diagrams which Use Oxides of Major and Minor Elements, *Lithos*, 1989, vol. 22, pp. 247–283.

Shaw, D.M., Trace Element Fractionation during Anatexis, *Geochim. Cosmochim. Acta*, 1970, vol. 34, pp. 237–243.

Shcheka, S.A., *Bazit-giperbazitovye intruzii i vklyucheniya v effuzivakh Dal'nego Vostoka* (Mafic–Ultramafic Intrusions and Xenoliths in Volcanics of the Far East), Moscow: Nauka, 1983.

Simkin, T. and Smith, J.V., Minor-Element Distribution in Olivine, *J. Geol.*, 1970, vol. 78, no. 3, pp. 247–283.

Smolkin, V.F., *Komatiitovyi i pikritovyi magmatizm rannego dokembriya Baltiiskogo shchita* (Komatiitic and Picritic Magmatism of the Early Precambrian in the Baltic Shield), St. Petersburg: Nauka, 1992.

Smolkin, V.F., Magmatism of the Early Proterozoic (2.5–1.7 Ga) Paleoriftogenic System in the Northwestern Baltic Shield, *Petrologiya*, 1997, vol. 5, no. 4, pp. 394–411.

Smolkin, V.F., Borisova, V.V., and Borisov, A.E., New Komatiite Find in the Kola Peninsula, *XVI Vsesoyuznyi seminar. Geokhimiya magmaticheskikh porod. Tez. dokl.* (Abstr. XVI All-Union Conf. on Geochemistry of Igneous Rocks), Moscow: Vernadsky Inst. Geokhim. Analit. Khim., Akad. Nauk SSSR, 1991, p. 110.

Smolkin, V.F., Borisova, V.V., and Vinogradov, A.N., Komatiite Association of the Kolmozero–Voron'ya Archean Belt, Kola Peninsula, *Izv. Akad. Nauk SSSR, Ser. Geol.*, 1991, no. 4, pp. 54–65.

Smolkin, V.F. and Pakhomovskii, Ya.A., Olivine–Chrome Spinel Mineral Assemblages in Ultramafic Rocks of Pechenga and Its Petrogenetic Importance, *Izv. Akad. Nauk SSSR, Ser. Geol.*, 1985, no. 4, pp. 57–73.

Snyder, G.A., Higgins, S.J., Taylor, L.A., *et al.*, Archean Enriched Mantle beneath the Baltic Shield: Rare-Earth-Element Evidence from the Burakovsky Layered Intrusion, Southern Karelia, Russia, *Int. Geol. Rev.*, 1996, vol. 38, pp. 389–404.

Stamateloupoulou-Seymour, K. and Francins, D.M., Metamorphic Olivine in Peridotitic Komatiite Flows, Lac Guyer, Quebec, *Contrib. Mineral. Petrol.*, 1980, vol. 18, no. 3, pp. 265–274.

Svetov, S.A., *Komatiit-toleitovye assotsiatsii Vedlozersko-Segozerskogo zelenokamennogo poyasa Tsentral'noi Karelii* (Komatiite–Tholeiite Associations of the Vedlozero–Segozero Greenstone Belt, Central Karelia), Petrozavodsk: Ross. Akad. Nauk, Karel'skii Nauch. Tsentr, 1997.

Vance, J.A. and Dungan, M.A., Formation of Peridotites by Deserpentinization in the Darrington and Sultan Areas, Cascade Mountains, Washington, *Geol. Soc. Am. Bull.*, 1977, vol. 8, no. 10, pp. 1497–1508.

Velinskii, V.V. and Bannikov, O.L., *Oliviny al'pinotipnykh giperbazitov* (Olivine in Alpine-Type Ultramafic Rocks), Novosibirsk: Nauka, 1986.

Vetrin, V.R., *Granitoidy Murmanskogo bloka* (Granitoids of the Murmansk Block), Apatity: Kol. Fil. Akad. Nauk SSSR, 1984.

Viljonen, M.J. and Viljonen, R.P., The Geology and Geochemistry of the Lower Ultramafic Unit of the

Onverwacht Group and Proposed New Class of Igneous Rocks, *Spec. Publ. Geol. Soc. S. Afr.*, 1969, no. 2, pp. 55–85.

Vrevsky, A.B. and Krymsky, R.Sh., Sm–Nd Systematics and Geochemistry of Archean Peridotitic Komatiites in the Baltic Shield, *Dokl. Ross. Akad. Nauk*, 1997, vol. 352, no. 1, pp. 80–82.

Vrevsky, A.B., Komatiites from the Early Precambrian Polmos–Poros Belt, Kola Peninsula, *Dokl. Akad. Nauk SSSR*, 1980, vol. 252, no. 3, pp. 1216–1219.

Vrevsky, A.B., *Petrologiya i geodinamicheskie rezhimy razvitiya arkheiskoi litosfery* (Petrology and Geochemical Regimes of the Evolution of the Archean Lithosphere), Leningrad: Nauka, 1989.

Vrevsky, A.B., Krymsky, R.Sh., and Svetov, S.A., Isotopic (Nd, O) and Geochemical (REE) Heterogeneity of the Archean Mantle, Baltic Shield, in *Precambrian Crust Evolution in the North Atlantic Region, Spec. Publ. Geol. Soc. London*, 1996, no. 112, pp. 34–48.

Zelenokamennye poyasa fundamenta Vostochno-Evropeiskoi platformy (geologiya i petrologiya vulkanitov) (Greenstone Belts in the Basement of the Eastern European Platform: Geology and Petrology of Volcanics), Lobach-Zhuchenko, S.B., Ed., Leningrad: Nauka, 1988.

Zhou, M. and Kerrich, R., Morphology and Composition of Chromite in Komatiites from the Belingwe Greenstone Belt, Zimbabwe, *Can. Mineral.*, 1992, vol. 30, pp. 303–317.